EJBCS

Eurasian Journal of Biological and Chemical Sciences (Eurasian J. Bio. Chem. Sci.)

Cilt:1 Volume: 2 Year: 2018

e-ISSN 2651-5237

EJBCS

Eurasian Journal of Biological and Chemical Sciences

Cilt: 1 Volume: 2 Year: 2018

Published Biannually

Corresponding Address
Gaziantep University, Faculty of Arts and Sciences, Department of Biology, Gaziantep, Turkey
E-mail: eurasianbiochemjournal@gmail.com / mtdogan1@gmail.com
Web: http://dergipark.gov.tr/ejbcs

Owner / Publisher
Dr. Muhammet DOĞAN
This journal is peer-reviewed and published twice (June, December) a year.

e-ISSN 2651-5237

Eurasian J. Bio. Chem. Sci. 1(2): 33-36, 2018

EJBCS

Eurasian Journal of Biological and Chemical Sciences

Journal homepage: www.dergipark.gov.tr/ejbcs

Determination of Phenolic Profile of *Cirsium arvense* (L.) Scop. Subsp. *vestitum* (Wimmer et Grab.) Petrak Plant

Ali Rıza TÜFEKÇİ[1*], Hüseyin AKŞİT[2], Fatih GÜL[1], İbrahim DEMİRTAŞ[1]

[1]*Cankiri Karatekin University, Science Faculty, Department of Chemistry, Cankiri, Turkey*

[2] *Erzincan University, Faculty of Pharmacy, Basic Pharmacy Sciences, Erzincan, Turkey*

*Corresponding author : alirizatufekci@gmail.com

Orcid No: 0000-0002-2951-3657

Abstract: The chemical composition and fatty acid contents of *Cirsium arvense* subsp. *vestitum* aerial parts (flowers (CaF) and stem-leaf (CaSL)) was examined in this study. Aerial parts of this plant were extracted with various solvents such as hexane (CaFH and CaSLH), chloroform (CaFC and CaSLC) and methanol / chloroform (CaFMC and CaSLMC). Fatty acid analysis of the hexane extracts was carried out by GC-MS and the phenolic content of other extracts were determined by HPLC-TOF/MS. Palmitic acid methyl ester composition in extract of CaFH (9.99%) and α-amyrenyl acetate compound in extract of CaSLH (23.13%) were founded as main components. Compared with other extracts, it was determined that the number and amount of components in the chloroform extract was very low. Content analysis of CaFMC and CaSLMC extracts revealed some differences and different components. In these extracts, apigenin and apigenin-7-*O*-β-D-glucuronide were determined as the major compounds. In addition, phenolic component analysis was performed for the first time on this plant species.

Keywords: *Cirsium arvense* subsp. *vestitum*, GC-MS, HPLC-TOF/MS, phenolic compounds

Cirsium arvense (L.) Scop. Subsp. vestitum (Wimmer et Grab.) Petrak bitkisinin Fenolik Profolinin Belirlenmesi

Özet: Bu çalışmada, *Cirsium arvense* subsp. *vestitum* bitkisinin toprak üstü kısımlarının (çiçek (CaF) ve gövde-yaprak (CaSL)) kimyasal bileşenleri ve yağ asidi içeriği incelenmiştir. Bu bitkinin toprak üstü kısımları hekzan (CaFH ve CaSLH), kloroform (CaFC ve CaSLC) ve metanol/kloroform (CaFMC ve CaSLMC) gibi değişik çözücüler ile ektrakte edildi. Hekzan ekstrelerinin yağ asidi analizi GC-MS cihazı ile gerçekleştirildi ve diğer ekstraktların fenolik içeriği HPLC-TOF / MS cihazı ile belirlendi. CaFH ekstresinde palmitic acid metil ester (9.99%) bileşiği ve CaSLH ekstresinde α-amyrenyl acetate (23.13%) bileşiği ana bileşenler olarak bulundu. Diğer ekstreler ile karşılaştırıldığında, kloroform ekstraktındaki bileşenlerin sayısının ve miktarının çok düşük olduğu belirlenmiştir. CaFMC ve CaSLMC ekstrelerinin içerik analizleri faklı bileşenleri ve bileşenler arasında bazı farklılıkların olduğunu ortaya çıkardı. Bu ekstreler içerinde, apigenin ve apigenin-7-*O*-β-D-glucuronide bileşikleri ana bileşen olarak belirlendi. İlave olarak bu bitki türü üzerinde ilk kez fenolik bileşen analizi gerçekleştirilmiştir.

Anahtar Kelimeler: *Cirsium arvense* subsp. *vestitum*, GC-MS, HPLC-TOF/MS, phenolic compounds

1. Introduction

Cirsium is belong to Asteracea family (Chabani et al. 2013). *Cirsium* that known as thistle in widespread throughout the world grows in Central Europe, Balkans, South Russia, Central Asia, East Anatolia, in subtropical and tropical regions. Generally it is perennial and inhabits humid meadows, near the roadside field, orchard and clay soils.

According to recent studies, there are more species than about 300 species (Güner et al. 2000). This genus is represented by 78 taxa at the species, subspecies and variety level, in Turkey (Yıldız et al. 2013).

Cirsium species is rich in secondary metabolites (Noh et al. 2013) and has biological activities like for healing of wounds (Raven and Edwards, 2001), antibacterial, antifungal (Khan et al. 2011), antioxidant, antidiabetic, anti-inflammatory, vasorelaxant, astringent, hepatoprotective and anticancer activities (Yildiz et al. 2013). In some countries, such as in Turkey, some *Cirsium* species are considered as edible plants.

C. arvense species are believed to be harmful in agricultural areas as they can reproduce and grow uncontrollably (Demirtaş et al. 2017). To our find out about the chemical content of this plant species. Therefore, in this study, we work on to investigate phytochemical contents and fatty acids composition of extracts from *C. arvense*.

2. Materials and Method

2.1. Plant materials

Cirsium arvense subsp. *vestitum* (*C. arvense*) was collected from Sivas, Karaçayır, on sixteenth miles of (GPS data: 39 51 29 North, 36 58 48 East 1568 m), in 2008 June, Turkey and identified by Prof. Dr. Neriman Özhatay. A voucher specimen (ISTE 85428) has been deposited at the Herbarium of Faculty of Pharmacy, Istanbul University.

2.2. Preparation of Extracts Using Different Solvents

The areal parts of *C. arvense* [flowers (CaF) and steams-leaves (CaSL)] were cut into small pieces with liquid nitrogen. Firstly, CaF and CaSL parts were extracted with hexane, after were extracted chloroform and the last were used methanol-chloroform (1:1, v/v) for three times at room temperature. Then extracts were filtered through Whatman No. 2 filter paper and concentrated to dryness under vacuum. The crude extracts were stored under adequate conditions until the time of analysis.

2.3. GC-MS Analysis

Fatty acid and volatile components analysis of CaFH and CaSLH extracts were carried by GC-MS performed on an Agilent Technologies model 7890 gas chromatograph equipped with a 5975 Triple Axis Detector Mass spectrometer. Analyzes were carried out using HP-5 ms capillary column (30 m x 250 m x 0.25 µm film thickness, 5%-phenylmethylpolysiloxane). Ultra-pure helium was used as a carrier gas at a flow rate of 1 ml/min, splitless 2 µL injections were used. Electron impact (EI) ion source were used at 70 eV. Injector, ion source and interface temperatures were 250, 250 and 270 °C. Oven temperature programme was arranged as follow: starting temperature was 100 °C. The temperature was kept at 100 °C for 10 min, then increased to 200 °C at a 10 °C/min rate, and held for 10 min, then 25 °C/min to 270 °C for 36 min, held for 20 min. Total run time is 84 min. Compounds in samples were identified comparing with those in the NIST and WİLEY search database. Mass spectra were recorded in the m/z 50–550 mass range.

For GC-MS analysis, approximately 40 mg of extracts was weighed. The extracts were dissolved by the addition of 3 mL of KOH solution prepared in 2 M methanol. 3 ml of hexane was added to the solution and vortexed for 2 minutes. After a few minutes of waiting, two phases were observed. The esterified and hexane-phase supernatant was carefully separated from the lower phase. Hexane parts placed in vials.

knowledge, there is only one report on biological activity that so far has not been able to

2.4. HPLC-TOF/MS Analysis

Phenolic components analysis of CaFC, CaFMC, CaSLC and CaSLMC extracts were determined by Agilent Technology of 1260 Infinity HPLC System coupled with 6210 Time of Flight (TOF) LC/MS detector and ZORBAX SB-C18 (4.6 x100mm, 3.5µm) column. The mobile phases consisted of the A (ultra pure water with 0.1% formic acid) and B (acetonitrile-HPLC grade). Flow rate was 0.6 mL min^{-1} and column temperature was 35°C. Injection volume was 10 µL. The solvent program was as follow: 0.min 10% B; 0-1.min 10% B; 1-20.min 50% B; 20-23.min 80% B; 23-25.min 10% B; 25-30. min 10% B. Ionization mode of HPLC-TOF/MS instrument was negative and operated with a nitrogen gas temperature of 325 °C, nitrogen gas flow of 10.0 L min^{-1}, nebulizer of 40 psi, capillary voltage of 4000 V and finally, fragmentor voltage of 175 V. For sample analysis, dried crude extracts (250 ppm) were dissolved in methanol. Samples were filtered passing through a PTFE (0.22 µm) filter by an injector to remove particulates.

Table 1. GC-MS results of *C. arvense* extracts (CaFH and CaSLH)

No	RT (min)	Compounds name	% Area	
			CaFH	CaSLH
1	17.16	1-Dodecene	0.03	-
2	17.29	Tetradecane	0.03	0.06
3	19.29	Lauric acid, methyl ester	0.83	-
4	20.20	Cetene	0.04	0.05
5	20.30	Hexadecane	0.11	0.15
6	22.13	Myristic acid, methyl ester	0.21	0.53
7	23.25	1-Octadecene	0.03	0.04
8	23.38	Octadecane	0.08	0.11
9	23.89	Pentadecanoic acid, methyl ester	0.08	0.14
10	24.19	Phytol, acetate	0.14	0.19
11	24.34	Hexahydrofarnesyl acetone	0.51	0.71
12	24.72	Phytol, acetate	0.02	0.03
13	25.14	3,7,11,15-Tetramethyl-2-hexadecen-1-ol	0.05	0.06
14	26.23	Palmitic acid, methyl ester	9.99	20.51
15	28.20	Palmitic acid, ethyl ester	0.05	0.41
16	28.34	Eicosane	0.04	-
17	29.25	Palmitic acid, isopropyl ester	0.10	0.10
18	29.35	Hexadecanoic acid, 15-methyl-,methyl ester	-	0.24
19	31.36	Linoleic acid, methyl ester	2.16	0.91
20	31.48	Linolenic acid, methyl ester	1.01	1.14
21	31.68	Phytol	1.73	2.58
22	31.88	Stearic acid, methyl ester	2.32	3.19
23	32.15	10-Nonadecenoic acid	0.06	0.19
24	32.76	1-Hexadecanol, 2-methyl-	0.04	0.06
25	32.82	Nonadecane	0.11	0.10
26	33.14	Nonadecanoic acid methyl ester	0.03	-
27	33.75	Octadecanoic acid, 2-methyl-,methyl ester	-	0.10
28	33.89	Heneicosane	1.55	0.13
29	34.01	2-Nonadecanone	0.18	-
30	34.21	Arachidic acid methyl ester	3.08	1.75
31	34.56	4,8,12,16-Tetramethylheptadecan-4-olide	-	0.06
32	34.93	Heptadecane, 9-hexyl-	0.19	0.15
33	35.27	Heneicosanoic acid, methyl ester	0.11	0.08
34	35.99	1-Eicosanol	0.17	0.24
35	36.04	Tetracosane	0.65	0.47
36	36.15	Erucic acid methyl ester	-	0.17
37	36.43	Behenic acid, methyl ester	2.67	2.24
38	37.29	Eicosane, 10-methyl-	0.11	0.25
39	37.74	Tricosanoic acid, methyl ester	-	0.25
40	38.75	Hexacosane	5.05	5.14
41	39.29	Lignoceric acid methyl ester	0.58	2.36
42	40.49	Heptacosane	0.48	0.32
43	42.71	Octacosane	9.62	5.87
44	43.54	Cerotic acid methyl ester	-	0.29
45	46.73	Ethanol, 2-(9-octadecenyloxy)-	-	0.16
46	48.70	Hentriacontane	2.57	1.34
47	59.14	β -Sitosterol	0.30	0.50
48	60.92	β-Amyrin	1.18	3.92
49	63.71	α-Amyrin	1.88	7.22
50	67.85	12-Oleanen-3-yl acetate	4.43	0.48
51	69.76	Lupeol acetate (Isomers)	0.41	3.38
52	70.59	Lupeol	1.75	-
53	71.09	α-Amyrenyl acetate	7.71	23.13
54	71.43	Lupeol acetate (Isomers)	5.95	1.70
55	78.86	Lupeol acetate (Isomers)	5.82	0.79
56	80.15	Lupeol acetate (Isomers)	2.50	6.03

For HPLC-TOF/MS analysis, about 2 mg was weighed from each extracts. On the extracts were dissolved by adding 2 ml of methanol and 1000 ppm stock solutions were prepared. From the stock solutions, 200 ppm new solutions were prepared and transferred to the vials and analysed.

3. Results

This study includes the phytochemical study on the aerial parts of the *Cirsium arvense* subsp. *vestitum* plant genus. The results of GC-MS analysis of the hexane fractions of the this plant are given in Table 1. In addition, the GC-MS chromatograms of both extracts are presented in Figure 1 and 2. Analysis of the phenolic components for other extracts were quantitatively performed on HPLC-TOF/MS and quantitative differences in the extracts are shown in Table 2. On the other hand, HPLC-TOF/MS chromatograms of these extracts are shown in Figure 3. 57 compounds were determined in the hexane extracts. Palmitic acid methyl ester and α-amyrenyl acetate were determined as main components in CaFH extract (9.99%) and CaSLH extract (23.13%), respectively.

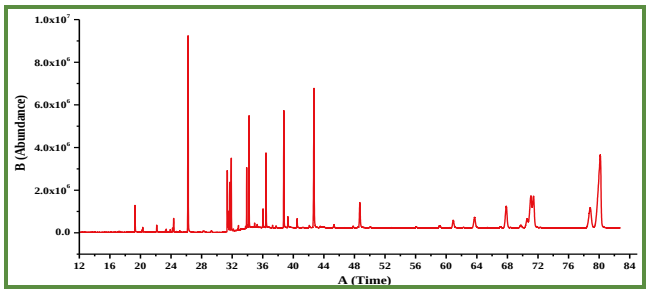

Figure 1. GC-MS chromatogram of CaFH

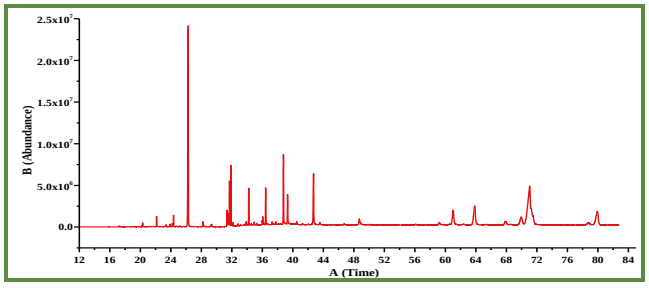

Figure 2. GC-MS chromatogram of CaSLH

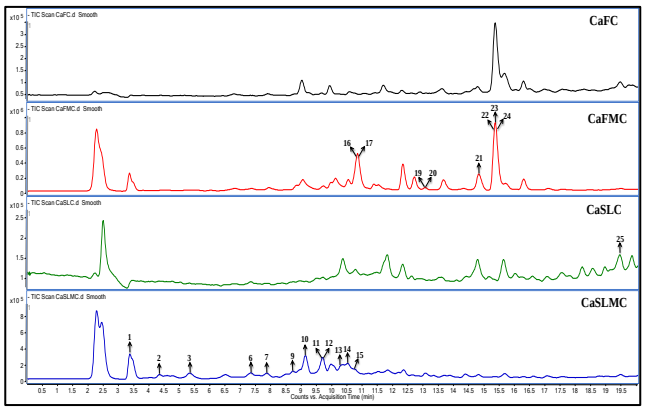

Figure 3. HPLC-TOF/MS TIC chromatogram of *C. arvense* extracts in negative ion mode

Table 2. Quantitative phenolic components of *C. arvense* plant extracts by HPLC-TOF/MS

No	Compounds name	RT	Results (mg phenolic / kg plant)			
			CaFC	CaFMC	CaSLC	CaSLMC
1	Fumaric acid	3.29		16.36		2.23
2	Gentisic acid	4.50		15.46	0.93	10.06
3	Chlorogenic acid	5.47		20.38	0.47	28.95
4	4-hidroxybenzoic acid	6.96	2.74	7.47	1.25	5.94
5	Protocatechuic acid	7.09		9.71		2.30
6	Caffeic acid	7.45		0.31		0.15
7	Vanillic acid	7.87	3.28	9.62	1.15	2.45
8	Syringic acid	8.08	4.08	13.07	1.90	2.53
9	Polydatine	8.61		1.12		
10	Rutin	9.24		21.93		43.88
11	Scutellarin	9.73		8.59		
12	Quercetin-3-β-D-glucoside	9.77		14.55		37.29
13	Naringin	10.50	0.30	6.21	3.17	4.99
14	Diosmin	10.62		31.95	3.56	6.37
15	Hesperidin	10.76				3.01
16	Apigetrin	10.79		65.10		
17	Apigenin-7-*O*-β-D-glucuronide	10.88		364.50		
18	Neohesperidin	11.08				3.31
19	Morin	13.01	1.91	7.95	1.15	2.45
20	Salicylic acid	13.11		0.35		
21	Cinnamic acid	15.16	1.42		0.92	
22	Diosmetin	15.36	7.66			
23	Naringenin	15.38		1.82		
24	Apigenin	15.39	54.23	558.80		1.48
25	Wogonin	19.46	9.91	17.17	8.21	7.80

Table 2 shows the results of the phenolic compounds contained in *C. arvense* plant extracts. The quantitative analysis of 25 compounds in the extracts were defined with HPLC-TOF/MS. It was determined that the compound number increased in the methanol/chloroform extract while the number of components in the chloroform extracts were very low. It has been determined that the CaFMC and CaSLMC extracts are present in different components, as well as are similar molecules. Rutin and Quercetin-3-β-D-glucoside compounds were found to be the main components of the CaSLMC extract while Apigenin and Apigenin-7-O-β-D-glucuronide compounds were the main components of CaFMC extract.

4. Discussion

Plants are capable of producing different fatty acids in different organs. The content analysis of the hexane extracts of *Cirsium arvense* subsp. *vestitum* plant shows differences from each other. This result indicates that fatty acids may be a chemo-taxonomical marker for plant species (Stuessy, 2009; Zhang et al. 2015). Palmitic, linoleic, and linolenic acids can have protective effect against hormone-dependent breast cancer. The protective mechanism involves the inhibition of aromatase activity, an enzyme participating in estrogen synthesis (Chen et al. 2006). Many *cirsium* species have got many compounds from the terpene class like steroids. The hexane extracts of this subspecies are rich in steroids-derived compounds. Steroids have many biological activities especially asthma treatment. For example, Ergosterol exhibits anti-inflammatory and anticancer effects (Barros et al. 2008). It has been scientifically determined that many steroids have a completely destructive effect on cancer cells such as HL-6, SF-295,

MDA-MB-435 and HCT-8 (Martucciello et al., 2018). Apigenin compound in CaFC, Apigenin-7-O-β-D-glucuronide compound in CaFMC extract, Wogonin compound in CaSLC extract and Rutin compound in CaSLMC extract are the most abundant compounds. In Demirtas and his co-workers' study in 2017, it is due to these compounds that cirsium arvense extracts show high activity against different cancer cells (Demirtaş et al. 2017). Rutin has some activities such as antibacterial, antitumor, anti-inflammatory, antiallergic and antioxidant in literature (Calabro et al. 2005).

5. Conclusions

Although the *Cirsium arvense* subsp. *vestitum* plant is considered to be an agricultural pest and idle plant among the population, our results show that aerial parts of this plant species contain very rich primer and secondary compounds. Besides, this plant species can be used as an odor and flavor in food and perfumery industry, but also because of its medical properties.

Acknowledgements

The authors thank to State Planning Organization, Turkey (DPT 2003K120510) for the financial support, University of Çankırı Karatekin for grant (BAP; FF28015B01).

References

Calabro M, Tommasini S, Donato P, Stancanelli R, Raneri D, Catania S, Ficarra R 2005. The rutin/β-cyclodextrin interactions in fully aqueous solution: spectroscopic studies and biological assays. J Pharmaceut Biomed 36(5): 1019-1027.

Chabanı S, Haba H, Lavaud C, Benkhaled M, Harakat D 2013. Flavonoid glycosides and triterpenoids from *Atractylis flava*. Phytochem Lett 6: 9–13.

Chen S, Oh SR, Phung S, Hur G, Ye JJ, Kwok SL 2006. Anti-aromatase activity of phytochemicals in white button mushrooms (Agaricus bisporus). Cancer Res 66: 12026–12034.

Demirtas I, Tufekci AR, Sahin Yaglioglu A, Elmastas M 2017. Studies on the antioxidant and antiproli ferative potentials of *Cirsium arvense* subsp. *vestitum*. J Food Biochem 41(1): 1-10.

Güner A, Özhatay FN, Ekim T, Başer KHC 2000. Flora of Turkey and the East Aegean Islands. Vol. 11 (Suppl. 2). Edinburgh: Edinburgh University Press.

Khan A, Amin A, Khan MA, Ali I 2011. In vitro screening of *Circium arvense* for potential antibacterial and antifungal activities. Pak J Pharm Sci 24: 519–522.

Martucciello S, Paolella G, Muzashvili TS, Skhirtladze A, Pizza C, Caputo I, Piacente S 2018. Steroids from Helleborus caucasicus reduce cancer cell viability inducing apoptosis and GRP78 down-regulation. Chem-Biol Interact 279: 43-50.

Noh H, Lee H, Kim E, Mu L, Rhee YK, Cho CW, Chung J 2013. Inhibitory effect of a *Cirsium setidens* extract on hepatic fat accumulation in mice fed a high-fat diet via the induction of fatty acid b-oxidation. Biosci Biotech Bioch 77: 1424–1429.

Raven JA, Edwards D 2001. Ristryoots: Evolutionary origins and biogeochemical significance. J Exp Bot 52: 381–401.

Stuessy TF 2009. Plant taxonomy, the systematic evaluation of comparative data. New York, NY, USA: Columbia University Press, 1–533.

Yıldız B, Arabacı T, Dirmenci T 2013. Two new species of *Cirsium* (Asteraceae) and notes on allies from Turkey. Turk J Bot 37: 1045–54.

Yıldız O, Can Z, Saral O, Yulu GE, Öztürk F, Alıyazıcıoğlu R, Canpolat S, Kolaylı S 2013. Hepatoprotective potential of chestnut Bee pollen on carbon tetrachloride-induced hepatic damages in rats. Evid-Based Compl Alt Available: doi.org/10.1155/2013/461478.

Zhang JL, Zhang SB, Zhang YP, Kitajima K 2015. Effects of phylogeny and climate on seed oil fatty acid composition across 747 plant species in China. Ind Crop Prod 63: 1–8.

Eurasian J. Bio. Chem. Sci. 1(2): 37-41, 2018

EJBCS

Eurasian Journal of Biological and Chemical Sciences

Journal homepage: www.dergipark.gov.tr/ejbcs

Examination of sulfamethoxazole, trimethoprim and dichlorophenac micropollutants along Sakarya River and treated by different ultrafiltration membranes

Fatma Büşra Yaman Büyükbüberoğlu [1*] Mehmet Çakmakçı[1]

[1] *Yıldız Teknik Üniversitesi, İnşaat Fakültesi, Çevre Mühendisliği Bölümü, İstanbul*

*Corresponding author : *fbyaman*@gmail.com

Abstract: In this study, The removal of micropollutants in the Sakarya River at five different locations and three different pharmaceuticals and water quality parameters are examined. To remove the micropollutants and improve the water quality, microfiltration (MF), and ultra-filtration (UF) membranes were used for treatment. Pharmacological pollutants, such as trimethoprim (TMP), sulfamethoxazole (SMX) and dichlorophanac (DFN) are chosed for treatment, which can be found in water very frequently and in high amounts. The best removal efficiency was obtained with UP005 UF membrane, it can be treated up to 66.

Keywords: sulfamethoxazole,trimethoprim and dichlorophanac,ultrafiltration membrane

Sakarya Nehri boyunca sülfametaksazol, trimetoprim ve diklorafenak mikrokirleticilerin incelenmesi ve farklı ultrafiltrayon membranlar ile arıtımı

Özet: Bu çalışmada Türkiye için önemli su kaynaklarından biri olan Sakarya Nehri boyunca 5 farklı noktadan numune alınarak sülfametaksazol, trimetoprim ve diklorafenak mikrokirleticileri ve çözünmüş organik karbon (ÇOK), ultraviolet absrobance at 254 nm dalga boyu (UV254), sertlik, iletkenlik gibi su kalite parametreleri incelenmiş, mikrokirleticilerin giderilmesi ve su kalitesinin iyileştirilmesi amacıyla mikrofiltrasyon (MF) ve ultrafiltrasyon (UF) membranları ile arıtım çalışmaları yapılmıştır. En iyi arıtma verimi UP005 UF membran ile elde edilmiştir. Küçük por çaplı ultrafiltrasyon membranlar ile; TMP, SMX ve DFN gibi sularda çok sıklıkla ve yüksek miktarlarda bulunabilen farmakolojik kirleticilerin %66 'ya kadar çıkabilen bir verimle arıtılabildiği görülmüştür.

Anahtar Kelimeler: : sülfametaksazol, trimetoprim ve diklorafenak, ultrafiltrasyon membran

1. Giriş

Son zamanlarda yapılan çalışmalarda tıbbi kaynaklı ilaçlar, pestisit gibi tarımsal alanda kullanılan ilaçlar ve kişisel bakım ürünleri gibi genel olarak mikrokirletici adı verilen kimyasalların içme suyu kaynağı olarak kullanılan sucul ortamlarda sıklıkla görülmeye başlanmıştır.(Alexander ve ark.,2012) Bu tip kirleticiler "öncelikli kirleticiler" olarak adlandırılmakta ve ng/L-µg/L gibi düşük konsantrasyonları bile sucul ortamdaki canlılar ve insan sağlığı açısından endişe verici olumsuz sonuçlara yol açmaktadır (Broséus ve ark.,2009; Shen ve Andrews, 2011).Tıp ve veterinerlik kullanımı sonucu 5000'den fazla ilaç doğaya karışmaktadır (Van Doorslaer ve ark.,2014). Avrupa Birliği (AB)'nde şu an kullanımda olan, farklı terapötik sınıflara ait çok farklı kimyasal özelliklerde, insani kullanım amaçlı yaklaşık 5000 farklı farmasötik madde bulunmaktadır (Wen ve ark.,2014). Son yıllarda yapılan araştırmalar sonucunda farmasötik maddelerin yüzey ve yeraltı sularında geniş bir dağılım gösterdiği görülmüştür Derco ve ark., 2015; Azzouz ve Ballesteros, 2013). Yüzeysel sularda, yeraltı sularında ve içme sularında 150'den fazla farmasötik madde tespit edilmiştir (Cristale ve ark., 2013).

Bu maddeler günlük kullanımdaki yüzlerce ilaç, deterjan, kişisel bakım, zirâi vb. ürünlerden kaynaklanmakta ve genel olarak bunlar literatürde PPCPs (pharmaceuticals and personal care products) olarak geçmektedir (Shen ve Andrews, 2011). Bu atıklar evsel,endüstriyel deşarjlar ile rögar, hastane, mezbaha, tarımsal alanlardan gelen yağmur

akışları ve yetersiz arıtma yapan atıksu arıtma tesislerinindeşarjları sonucu su kütlelerine karışabilmektedirler. Şekil 1 (a) 'da kirleticilerin doğaya karışım döngüsü verilmiştir.

Su ortamında en büyük endişe ilaç grubunda bulunan antibiyotiklerden kaynaklanmaktadır (Johnson ve ark., 2015). Antibiyotikler çok düşük konsantrasyonlarda bile alg çeşitliliğini azaltmakta ve bakteri direncini artırarak sucul yaşamı olumsuz etkilemektedir (Zhang ve ark., 2016). Antibiyotikler yüksek dayanım güçleri sebebiyle bozunmadan uzun süre alıcı ortamda kalabilmektedirler (Van Doorslaer ve ark., 2014).

Sülfametaksazol (SMX) ve Trimetoprim (TMP) ilaçları bronşit ve idrar yolu enfeksiyonlarının tedavisinde genellikle beraber olarak kullanılmaktadır (Daneshvar ve ark.,2012). Beraber kullanıldıklarında birbirinin etkisini artırmaktadır. Bu ilaçlar veterinerlik alanında da kullanılmaktadır (Yang ve ark.,2014; Peng ve ark.,2016).

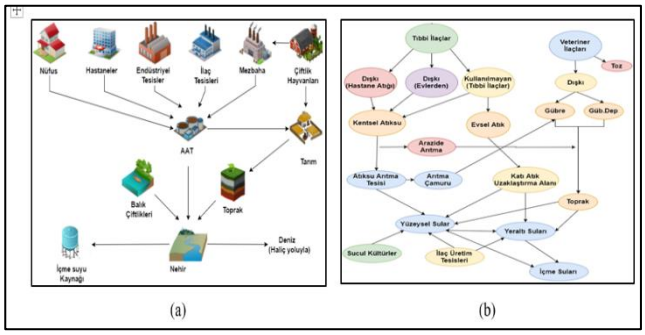

Şekil 1. Kirleticilerin doğaya karışım şekilleri

SMX tetrahydrafolik asit sentezleyen enzimleri inhibe eder, TMP ise tetrahydrafolik asiti yok etmek için farklı bir enzim salgılar. Bu sebeple bu iki ilaç 1960'dan beri beraber kullanılmaktadır (Dias ve ark.,2014; Johnson ve ark.,2015; Peng ve ark.,2016). TMP ve SMP konvansiyonel atıksu arıtma tesislerinde tamamen arıtılamamakta, yüzeysel sulara kadar ulaşmaktadır (Yang ve ark.,2015; Zheng ve ark.,2015). Su ortamında SMX'lerin sucul ortamlarda yaygın olarak görülmesi potansiyel ekotoksik etkisi ve bakterilere karşı yüksek dirence sahip olmalarından dolayı büyük endişe oluşturmaktadır (Dias ve ark.,2014). Barnes ve ark.(2008) yaptığı çalışmada yüzeysel sularda SMX'in 1,11 mg/L'ye kadar çıktığını belirtmişlerdir. Loos ve ark.(2009) alıcı ortamda SMX'in maksimum 4 mg/L olduğunu görmüşlerdir TMP'nin atıksu arıtma tesisi çıkışında 0,003 to 4,30 µg/L konsantrasyon aralığında olduğu ve bu konsantrasyonun yüzeysel sulara deşarj edildiği belirtilmiştir.

Diklorafenak (DCF) reçete olmadan satılan en yaygın nonsteroid antiinflamatuvar ilaçlardan biridir, Avrupa'da yılda yaklaşık 100 ton satılmaktadır. (Esteban ve ark., 2016; Lu ve ark.,2016). DCF suda yaşayan canlılar ve bitkiler üzerinde toksik etkiye sahiptir aynı zamanda insanlarda da hemodinamik değişiklikler ve tiroid tümörlerine neden olduğu belirtilmiştir. DCF'nin tüketildikten sonra %15'i değişmeden doğaya karışmaktadır. DCF biyolojik olarak birikme eğilimi göstermektedir ve başka ilaçlar ile birleşerek toksik etkisi önemli derecede artmaktadır (Bhadra ve ark., 2016). Atıksu arıtma tesislerinde konvansiyonel arıtımla DCF tam olarak arıtılamadığı için alıcı su ortamlarında da en sık saptanan kirleticilerden biridir (Perisic ve ark., 2016). Félix–Cañedo ve ark. (2013) yaptıkları çalışmada yüzeysel sularda DCF konsantrayonunun 28-32 ng/L olduğunu belirtmişlerdir. Bazı çalışmalarda da yüzeysel sularda 1-310 ng/L gibi geniş bir konsantrasyon aralığında bulunduğu belirtilmiştir.(Chong, ve ark., 2017; Félix–Cañedo ve ark., 2013).

Mikrokirleticilerin yüzeysel ve yeraltı sularından arıtımı her geçen gün daha çok önem kazanmaktadır. Amerika'da ve Avrupa ülkelerinde yapılan çeşitli araştırmalarda yüzeysel ve yeraltı sularında ve hatta arıtma tesisi çıkış sularında, 300'ün üzerinde mikrokirleticiye rastlandığı bildirilmiştir. Özellikle tıbbi ilaçlar insan metabolizmasından dışkı ve idrarla ilaç kalıntıları olarak veya ana madde olarak atılmakta ve sucul sistemlere çeşitli yollarla ulaşmaktadırlar (Şekil 1(b)). Bütün bu sebeplerden dolayı her geçen gün mikrokirletici arıtımı önem kazanmaktadır. Son zamanlarda yapılan çalışmalar; koagülasyon/flokülasyon, filltrasyon, klorlama gibi sistemleri içeren klasik (konvansiyonel) içme suyu arıtma tesislerinin mikrokirletici gideriminde etkisiz olduğu belirtilmiş ve ileri arıtım yöntemlerinin uygulanması gerektiği vurgulamıştır (Broséus ve ark.,2009;Félix–Cañedo ve ark.,2013).

2. Materyal ve Metot

2.1. Numune Alma Noktaları

Çalışmada Sakarya Nehri boyunca 5 farklı noktadan numune alınmıştır. Ilk nokta Sakarya nehrinin doğduğu nokta olan Çiftelerdir. İkinci ve üçüncü noktalar sırasıyla Gökçekaya ve Yenice barajlarıdır. Dördüncü nokta olarak yerleşmenin ve sanayinin yoğun olduğu bir bölge olan Geyve seçilmiştir. Son numune alma noktası ise Sakarya Nehrinin Karadeniz'e döküldüğü nokta olan Karasu bölgesidir. Böylelikle nehir boyunca doğduğu noktadan denize döküldüğü noktaya kadar hem yüksek kirlilik içermesi (Geyve gibi) hem de yüksek kalitede olması beklenen noktalardan (Gökçekaya ve Yenice barajları gibi) numune alınarak su kalitesi izlenmiş olacaktır. Numune alma noktaları Şekil 2'de görülmektedir.

Şekil 2. Numune alma noktalarının haritadaki konumu

2.2 Deneysel Yöntem

Ham su analizi Tablo 1 'de ve yöntemleri ile verilmiştir

Çizelge 1. Karakterizasyon için ölçülen parametreler

Parametre	Yöntem	Ekipman
TOK	SM 5310 B	TOK Ölçüm Cihazı
ÇOK	SM 5310 B	TOK Ölçüm Cihazı
UV_{254}	SM 5910	UV-visible spektrofotometresi
$SUVA_{254}$	Hesap yolu ile belirlenecektir.	Hesap yolu ile belirlenecektir.
Serbest Klor	SM 4500 Cl	Kimyasal analizle
Bulanıklık	SM 2130 B	Türbidimetre
İletkenlik	SM 2510	İletkenlik elektrodu
pH	SM 4500 H	pH elektodu
ÇO	SM 4500 G	ÇO elektrodu
Sıcaklık	SM 2550	Sıcaklık elektrodu
Ağır metaller	3111 B	Atomik absorbsiyon spektrofotometresi
İyonlar	SM 4140	İyon Kromotografi
Toplam sertlik	SM 2340 C	Kimyasal analizle
Alkalinite	SM 2320 B	Kimyasal analizle
Mangan	3111 B	Atomik absorbsiyon spektrofotometresi
Toplam sertlik	SM 2340 C	Kimyasal analizle

2.3 Membran Deney Düzeneği

Ham suların süzülmesi amacıyla Şekil 3'de gösterilen Amicon 8400 membran düzeneği kullanılmıştır. Karıştırmalı süzme düzeneğinde bulunan membran hücresinin hacmi 400 ml ve çapı ise 76 mm'dir. Sistem işletilirken magnet manyetik karıştırıcı ile döndürülmekte ve membran yüzeyinde dik filtrasyon sebebiyle oluşabilecek birikim engellenmektedir. Böylece sistem çapraz akışlı düzeneğe benzer şekilde işletilmiştir. Membran hücresinde istenilen basınç değeri azot gazı ile oluşturulmaktadır.

Şekil 3. Membran deney düzeneği

3. Bulgular ve Tartışma

Sakarya Nehrinden numune ilkbahar mevsiminde (Mart 2015'de) alınmıştır. Tablo 2'de su karakterizasyonu verilmiştir. Numunelerin ortalama pH, sıcaklık ve iletkenlik değerleri sırasıyla 7,76, 9,04 0C, 901 µS/cm olarak ölçülmüştür. pH ve sıcaklık parametreleri açısından sular 5 noktada da Yüzeysel Su Kalitesi Yönetimi Yönetmeliği (YSKYY)'ne 1. Sınıf su özelliği gösterirken, İçme suyu Elde Edilen veya Elde Edilmesi Planlanan e Yüzeysel Suların Kalitesine Dair Yönetmelik](İSEEPSHY)'e göre de A1 sınıfına girmektedir. İletkenlik değerlerine göre Geyve 3. Sınıf Çifteler, Gökçekaya, Yenice ve Karasu ise 2. sınıf su özelliği taşımaktadır.

Çizelge 2. Sakarya Nehrine ait su karakterizasyonu

Deney Adı	Çifteler	Gökçekaya	Yenice	Geyve	Karasu	TS266	EPA
pH	7,83	7,86	7,88	7,98	7,28	9,5-6.5	6.6-8.5
Sıcaklık (^{0}C)	14,4	15,2	12,28	16,3	14,5	-	-
İletkenlik (µS/cm)	795	858	845	1012	988	2500	-
Çözünmüş oksijen (mg O_2/L)	7,2	6,9	7,54	7,93	7,2	-	-
AKM (mg/L)	20	26	28	32	24	-	-
Bulanıklık(NTU)	10,22	11,63	15	20,12	18,00	-	-
Nitrat (mg NO_3/L)	0,32	0,86	0,81	0,99	0,78	0,5	45
Florür (mg F/L)	0,61	0,62	0,19	0,11	0,17	1,50	2
Bromür (mg /L)	0,08	0,17	0,17	0,18	0,07		1
Demir (mg Fe/L)	< 0,25	< 0,25	< 0,25	< 0,25	< 0,25	0,2	0,2
Mangan (mg Mn/L)	< 0,2	< 0,2	< 0,2	< 0,2	< 0,2	0,05	0,05
Bakır (mg Cu/L)	< 0,25	< 0,25	< 0,25	< 0,25	< 0,25	-	2
Çinko (mg Zn/L)	0,129	<0,1	<0,1	<0,1	<0,1	-	5
Nikel (mg Ni/L)	<0,5	<0,5	<0,5	<0,5	<0,5	0,002	0,002
Kadmiyum (mg Cd/L)	<0,1	<0,1	<0,1	<0,1	<0,1	0,005	0,005
Toplam krom (mg Cr/L)	<2	<2	<2	<2	<2	0,005	0,05
Kurşun (mg Pb/L)	<1	<1	<1	<1	<1	0,01	0,015
Sülfat (mg SO_4/L)	187	189	140	97	128	250	250
Klorür (mg Cl/L)	21,99	87,47	84,9	57,48	40	250	250
UV_{254} (cm -1)	0,026	0,104	0,198	0,185	0,137	-	-
TOK (mg/L)	9,72	10,12	11,6	13,62	12,4	-	-
$SUVA_{254}$	0,27	0,87	1,71	1,27	1,1	-	-
Alkalinite(mg $CaCO_3$/L)	330	260	255	250	265	-	-
Sertlik (mg $CaCO_3$/L)	464	400	386	348	328	-	-
Sülfametaksazol (ng/L)	0	17,6	31,2	15,2	13,2	-	-
Trimetoprim (ng/L)	0	2,1	1,5	0	0	-	-
Diklorafenak (ng/L)	13,26	0,4	1,2	0,2	0,4	-	-

Organik madde giderimi için numunelerin UV_{254} ve ÇOK giderim verimleri kıyaslanmıştır. Şekil 4.'de UV_{254}, ÇOK, giderim verimleri verilmiştir. En yüksek UV_{254} giderimi UP005 membranı ile %46 ile Geyve'de elde edilirken en düşük UV_{254} giderimi ise %13 ile Çifteler ve Gökçekaya'da MV020 membranı ile elde edilmiştir. ÇOK giderim verimleri ise en düşük MV020 membran ile %10 Çifteler'de, en yüksek giderim verim ise UP005 membran ile %61 Geyve'de görülmüştür. UP020 membranında görülen en düşük ve en yüksek ÇOK giderim verimi ise sırasıyla %15 Çifteler ve %29 Gökçekaya'da görülmüştür. Sutherland ve ark.(2015) tarafından yapılan çalışmalarda <10 kDa UF membranlar ile 37-87% arasında ÇOK giderimi sağlanmıştır. Bu çalışmada da membranların gözenek boyutu veya moleküler ağırlığı azaldıkça organik madde giderme verimi artmıştır.

Şekil 5 'de Mikrokirleticilerin membran ile giderim verimi verilmiştir. MV020 membran ile her üç kirletici için giderim veriminin %1 ile %2 arasında olduğu ve mikrofiltrasyon membran ile mikrokirleticilerin gideriminin yok denecek kadar az olduğu görülmüştür. En yüksek giderim %66 ile Karasu ve Çifteler 'de UP005 membran ile SMX 'de görülürken onu %63 ve %61 ile Geyve ve Gökçekaya takip etmiştir. UP005 membran ile TMP 'nin arıtım verimi %59 ile %46 DFN 'nin ise %55 ile %44 arasında bulunmuştur. UP020 membran ile ise giderim

%21 ve %12 arasında değişim göstermiştir. Küçük por çaplı ultrafiltrasyon membranlar ile TMP, SMX ve DFN gibi sularda çok sıklıkla ve yüksek miktarlarda bulunabilen farmakolojik kirleticilerin %66 'ya kadar çıkabilen bir verimle arıtılabildiği görülmüştür.

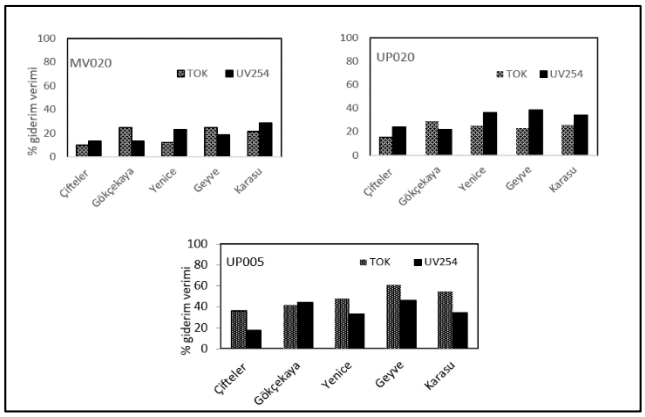

Şekil 4. Organik maddelerin membran ile giderim verimi

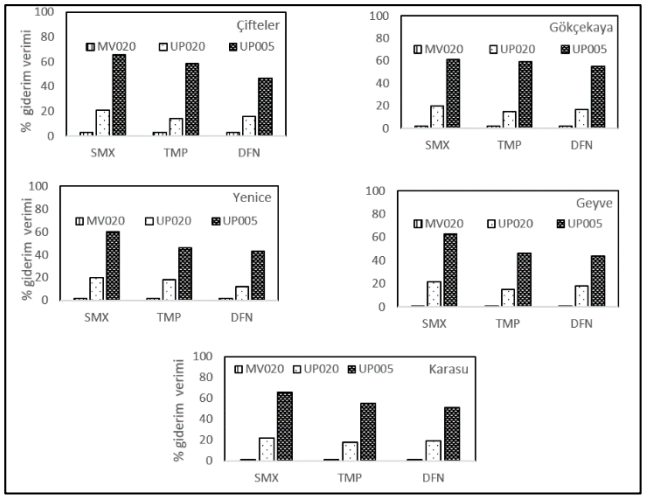

Şekil 5. Mikrokirleticilerin membran ile giderim verimi

4. Sonuç

Türkiye'nin dördüncü büyük su kaynağı olan Sakarya Nehri boyunca nehrin doğduğu ve denize döküldüğü noktaya kadar 5 farklı noktadan dört farklı mevsimde numune alınarak karakterizasyon ve SMX, TMP, ve DFN giderimi çalışılmıştır. Su Kalitesi Kontrol yönetmeliği su kalitesi sınıflarına göre Sakarya Nehri pH açısından 1. Sınıf iletkenlik açısından Geyve'de 3. Sınıf diğer noktalarda ise 2. su özelliği göstermektedir. Su karakterizasyonlarına göre Sakarya Nehiri'nin en temiz noktası nehrin doğduğu nokta olan Çifteler ve en kirli nokta ise sanayilerin ve yerleşimin yoğun olarak bulunduğu Geyve'dir. Bu çalışmada ilk defa Sakarya Nehri'nde mikrokirleticiler nehir boyunca incelenmiştir. Hem en yüksek organik madde hem de en yüksek mikrokirletici giderimin UP005 membran ile olduğu görülmüştür.

Sakarya Nehri içme suyu kaynağı olarak kullanılması durumunda ilk tercih edilecek noktanın Çifteler olması gerekmektedir. Diğer noktalar veya yakın civarlarından su alınacak ise ızgaralar, biriktirme yapısı, konvansiyonel arıtma ve sonrasında ise membran ile arıtım tercih edilmelidir. Geyve ve Karasu noktasında nehrin kirlendiği göz önüne alınırsa bu noktalardaki yerleşim yerlerinin ve kontrolsüz deşarj yapabilecek noktaların denetlenmesi ve gerekli önemlerin alınması gerekmektedir.

Teşekkür

Bu Çalışma YTÜ Bilimsel Araştırma Projeleri Koordinatörlüğü (BAPK) tarafından desteklenmiş olup (2015-05-02-DOP03), koordinatörlük çalışanlarına da proje faaliyetleriyle ilgili yardımlarından dolayı teşekkür ederim. Deneysel çalışmalar aşamasında desteklerini esirgemeyen Ebubekir YÜKSEL'e teşekkürlerimi sunarım.

Kaynaklar

Alexander JT. Hai F I, Al-Aboud TM 2012. Chemical coagulation-based processes for trace organic contaminant removal: current state and future potential, J Environ Manage, 111: 195-207.

An Y, Wang Z, Wu Z, Yang D, Zhou Q 2009. Characterization of membrane foulants in an anaerobic non-woven fabric membrane bioreactor for municipal wastewater treatment, Chemical Engineering Journal, 155: 709-715.

Azzouz A ve Ballesteros E 2013. Influence of seasonal climate differences on the pharmaceutical, hormone and personal care product removal efficiency of a drinking water treatment plant, Chemosphere, 93: 2046-2054.

Barnes KK, Kolpin, DW, Furlong ET, Zaugg SD, Meyer MT, Barber LB 2008. A national reconnaissance of pharmaceuticals and other organic wastewater contaminants in the United States--I) groundwater", Sci Total Environ, 402: 192-200.

Bhadra BN, Seo PW, Jhung SH, 2016 Adsorption of diclofenac sodium from water using oxidized activated carbon, Chemical Engineering Journal, 301: 27-34.

Broséus R. Vincent S, Aboulfadl K, Daneshvar A, Sauvé S, Barbeau B, Prévost M 2009. Ozone oxidation of pharmaceuticals, endocrine disruptors and pesticides during drinking water treatment, Water Res, 43: 4707-4717.

Chong S, Zhang G, Wei Z, Zhang N, Huang T, Liu Y 2017. Sonocatalytic degradation of diclofenac with FeCeOx particles in water", Ultrasonics Sonochemistry, 34: 418-425.

Cristale J, Katsoyiannis A, Sweetman AJ, Jones KC, Lacorte S 2013. Occurrence and risk assessment of organophosphorus and brominated flame retardants in the River Aire (UK), Environ Pollut, 179: 194-200.

Daneshvar A, Aboulfadl K, Viglino L, Broseus R, Sauve S, Madoux-Humery AS., Weyhenmeyer GA, Prevost M. 2012 Evaluating pharmaceuticals and caffeine as indicators of fecal contamination in drinking water sources of the Greater Montreal region, Chemosphere, 88: 131-139.

Derco J, Dudáš J, Valičková M, Šimovičová K, Kecskés J 2015. Removal of micropollutants by ozone based processes,

Chemical Engineering and Processing: Process Intensification, 94: 78-84.

Dias, IN, Souza BS, Pereira JHOS, Moreira FC, Dezotti M, Boaventura RAR, Vilar VJP 2014. Enhancement of the photo-Fenton reaction at near neutral pH through the use of ferrioxalate complexes: A case study on trimethoprim and sulfamethoxazole antibiotics removal from aqueous solutions, Chemical Engineering Journal, 247: 302-313.

Drinking Water Contaminants – Standards and Regulations: EPA 2003.

Esteban S, Moreno-Merino L, Matellanes R, Catalá M, Gorga M, Petrovic M, López de Alda M, Barceló D Silva A, Durán J, López-Martínez J, Valcárcel Y, 2016 Presence of endocrine disruptors in freshwater in the northern Antarctic Peninsula region, Environ Res, 147: 179-192.

Félix–Cañedo TE, Durán–Álvarez JC, Jiménez–Cisneros B 2013 The occurrence and distribution of a group of organic micropollutants in Mexico City's water sources, Science of The Total Environment, 454-455: 109-118.

Fu G,Peng J, Wang Y, Zhao S, Fang W, Hu K, Shen J, Yao J 2016. Pharmacokinetics and pharmacodynamics of sulfamethoxazole and trimethoprim in swimming crabs (Portunus trituberculatus) and in vitro antibacterial activity against Vibrio: PK/PD of SMZ-TMP in crabs and antibacterial activity against Vibrio, Environmental Toxicology and Pharmacology, 46: 45-54.

İçmesuyu Elde Edilen veya Elde Edilmesi Planlanan Yüzeysel Suların Kalitesine Dair Yönetmelik Orman ve Su İşleri Bakanlığı, (29 Haziran 2012).

Johnson AC, Keller V, Dumont E, Sumpter JP. 2015. Assessing the concentrations and risks of toxicity from the antibiotics ciprofloxacin, sulfamethoxazole, trimethoprim and erythromycin in European rivers Sci Total Environ, 511: 747-755.

Loos R, Gawlik BM, Locoro G, Rimaviciute E, Contini S, Bidoglio G 2009 EU-wide survey of polar organic persistent pollutants in European river waters, Environ Pollut, 157: 561-568.

Lu X, Shao Y, Gao N, Chen J, Zhang Y, Wang Q,mLu Y 2016 Adsorption and removal of clofibric acid and diclofenac from water with MIEX resin", Chemosphere, 161: 400-411.

Perisic DJ. Gilja V, Stankov MN. Katancic Z, Kusic H, Stangar UL, Dionysiou DD, Bozic AL 2016 Removal of diclofenac from water by zeolite-assisted advanced oxidation processes, Journal of Photochemistry and Photobiology A: Chemistry, 321: 238-247.

Petrie B., Barden R, Kasprzyk-Hordern B 2015 A review on emerging contaminants in wastewaters and the environment: Current knowledge, understudied areas and recommendations for future monitoring, Water Res, 72: 3-27.

Rivera-Utrilla J, Daiem MM, Sanchez-Polo M, Ocampo-Perez R, Lopez-Penalver, JJ, Velo-Gala I, Mota AJ 2016 Removal of compounds used as plasticizers and herbicides from water by means of gamma irradiation, Sci Total Environ, 569-570: 518-526.

Shen R ve Andrews SA 2011. Demonstration of 20 pharmaceuticals and personal care products (PPCPs) as nitrosamine precursors during chloramine disinfection, Water Res, 45: 944-952.

Su T, Deng H, Benskin JP, Radke M, 2016 Biodegradation of sulfamethoxazole photo-transformation products in a water/sediment test, Chemosphere, 148: 518-525.

Sutherland S, Parsons SA, Daneshkhah A, Jarvis P, Judd SJ 2015 THM precursor rejection by UF membranes treating Scottish surface waters. Separation and Purification Technology, 149: 381-388.

TS266 Standartları - İnsanî Tüketim Amaçlı Sular. 2005.

Van Doorslaer X, Dewulf J, Van Langenhove H, Demeestere K 2014. Fluoroquinolone antibiotics: An emerging class of environmental micropollutants, Science of The Total Environment, 500-501: 250-269.

Van Doorslaer X. Dewulf J, Van Langenhove H, Demeestere K, 2014 Fluoroquinolone antibiotics: An emerging class of environmental micropollutants, Science of The Total Environment, 500-501: 250-269.

Wang Z, Wu Z, Yin X, Tian L, 2008. Membrane fouling in a submerged membrane bioreactor (MBR) under sub-critical flux operation: Membrane foulant and gel layer characterization, Journal of Membrane Science, 325: 238-244.

Wang Z. Chen Z, Chang J, Shen J. Kang J, Chen Q 2015 Fabrication of a low-cost cementitious catalytic membrane for p-chloronitro benzene degradation using a hybrid ozonation-membrane filtration system", Chemical Engineering Journal, 262: 904-912.

Wen ZH, Chen L. Meng XZ, Duan YP, Zhang ZS, Zeng EY, 2014 Occurrence and human health risk of wastewater-derived pharmaceuticals in a drinking water source for Shanghai, East China, Sci Total Environ, 490: 987-993.

Yang GC, Yen CH, Wang CL, 2014. Monitoring and removal of residual phthalate esters and pharmaceuticals in the drinking water of Kaohsiung City, Taiwan, J Hazard Mater, 277: 53-61.

Yang L, Kim D, Uzun H. Karanfil T, Hur J.2015 Assessing trihalomethanes (THMs) and N-nitrosodimethylamine (NDMA) formation potentials in drinking water treatment plants using fluorescence spectroscopy and parallel factor analysis, Chemosphere, 121: 84-91.

Yüzeysel Su Kalitesi Yönetimi Yönetmeliği, Ankara: Orman ve Su İşleri Bakanlığı, (30 Kasım 2012).

Zhang Y, Wang A, Tian X, Wen Z, Li D, Li J. 2016 Efficient mineralization of the antibiotic trimethoprim by solar assisted photoelectro-Fenton process driven by a photovoltaic cell, J Hazard Mater, 318: 319-328.

Zheng D, Andrews RC, Andrews SA, Taylor-Edmonds L, 2015 Effects of coagulation on the removal of natural organic matter, genotoxicity, and precursors to halogenated furanones, Water Res, 70: 118-129.

Eurasian J. Bio. Chem. Sci. 1(2): 42-47, 2018

EJBCS

Eurasian Journal of Biological and Chemical Sciences

Journal homepage: www.dergipark.gov.tr/ejbcs

Thermal Characteristics and Kinetic Parameters Assessment of Chitosan

Sevgi Polat[1]*, Perviz Sayan[1]

[1]*Marmara University, Faculty of Engineering, Department of Chemical Engineering, Istanbul, Turkey*

*Corresponding author : sevgi.polat@marmara.edu.tr
Orcid No: 0000-0002-0934-2125

Abstract: In the present study, thermal decomposition kinetics of chitosan was investigated by a thermal analyzer. Firstly, the experiments were performed at three different heating rates from 30 °C to 800 °C under inert N_2 atmosphere. The results showed that the heating rate significantly affected the maximum peak temperature but it did not affect the conversion. When the heating rate increased, the maximum peak temperature shifted towards the higher temperature region. In the second part, the obtained thermal data was used to calculate the activation energies based on Flynn-Wall-Ozawa (FWO), Kissinger-Akahira-Sunose (KAS), Starink and Tang kinetic models. All models used provided accurate fits of experimental data and yielded acceptable errors. The values of the average activation energy for FWO, KAS, Starink and Tang models were determined to be 148.5, 146.4, 148.3 and 146.7 kJ/mol, respectively.

Keywords: Chitosan, Kinetics, Thermal decomposition, Model free

1. Introduction

Chitosan is a natural polysaccharide biopolymer and it is widely used in the biotechnology, biomedicine, food, agriculture and cosmetics industries (Kast et al. 2002; Lozano-Navarro et al. 2018). The use of chitosan is generally preferred due to its widespread availability, hydrophilicity, biocompatibility, non-toxicity, cost effectiveness, antibacterial properties and immune-stimulatory activities (Qu et al. 2000; Hamedi et al. 2018). Moreover, since chitosan is a kind of environment-friendly polymer material, its recycling in nature is often of primary interest to the scientific community, to understand its thermal decomposition. Its degradation in various environmental conditions causes to a destruction of chains by breaking, splitting of fragments of the main chain or side constituents and release of volatile products. The knowledge of its thermal kinetics may help better understanding and planning of its industrial processes because the adequate kinetic description of chemical and physical processes can be profitably applied for process design and optimization, and valid predictions (Zhou et al. 2009).

Thermogravimetric analysis (TGA) is one of the most common techniques, which allows obtaining reliable data to investigate thermal events and kinetics during decomposition of the materials. The kinetics of the thermal events have been determined by the application of the different kinetic models. Also, thermal decomposition in thermogravimetric analysis gives clues about the thermal behaviors at different temperature regions for the decomposition process. In the current study, thermal decomposition of the chitosan was performed using the thermogravimetric analyzer. From the obtained TGA data, the kinetic parameter such as activation energy for the thermal decomposition process of the chitosan was calculated.

2. Materials and Method

Chitosan used in this study was provided from Sigma-Aldrich Chemical Company and was of reagent grade. Thermogravimetric analysis experiments were performed by using the Setaram Labsys Evo instrument. 10 ± 0.5 mg of the sample was taken in Al_2O_3 crucible and the measurements were performed under a constant N_2 flow rate of 25 cm^3/min from 30 °C to 800 °C at heating rates of 5, 10 and 20 °C/min. The nitrogen flow ensured an inert atmosphere on the sample during the run, while the small amount of sample and the slow heating rate ensured that the heat transfer limitations can be ignored. From this analysis, thermogravimetric (TG) and differential thermogravimetric (DTG) curves were obtained and the experimental data was used to calculate the activation energy based on FWO, KAS, Starink, and Tang kinetic models.

3. Results and Discussion

3.1. TG/DTG Analysis

The TG and DTG curves obtained at different heating rates are shown in Figure 1. Based on these curves, two stages

can be observed during the thermal decomposition of the chitosan.

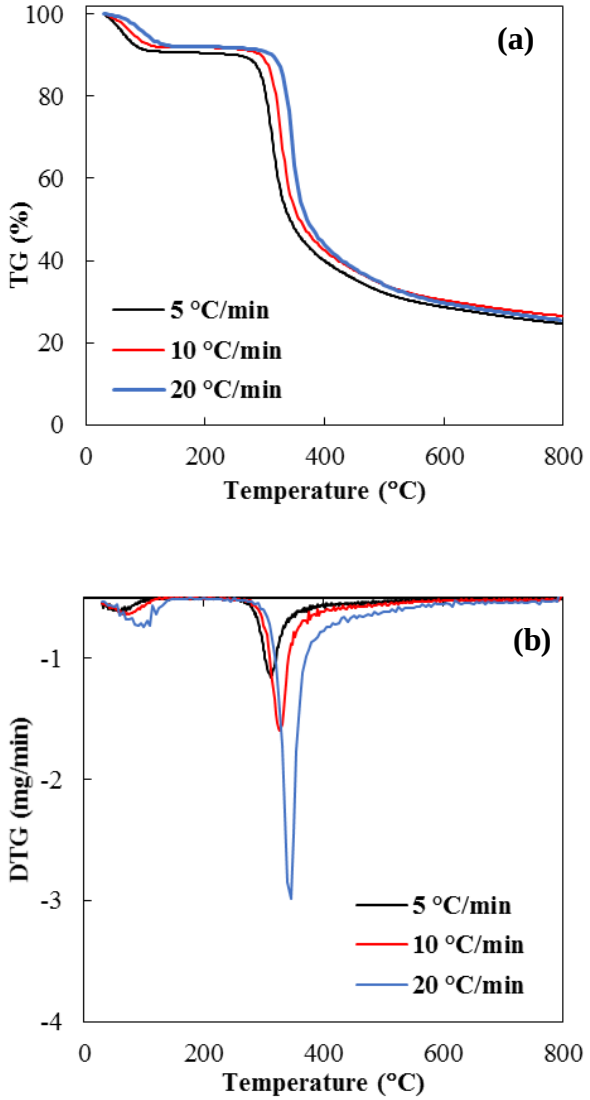

Figure 1. TG (a) and DTG (b) curves of chitosan at different heating rates

In the first stage occurring at temperature about 100 °C represented the evaporation of adsorbed water in the inner polymer. The total weight loss was about 10% of the initial weight and this value was almost the same for all heating rates. After the water removal, the main structure started to decompose due to increasing temperature. The curves indicated that the main decomposition zones were in the temperature range of 265-373, 285-380 and 300-400 °C for 5, 10 and 20 °C/min heating rates, respectively. The decomposition related to the deacetylation and depolymerization of the chitosan with the approximately 50% weight loss (Moussout et al. 2016; Moussout et al., 2018). When the DTG curves showing the reaction zone where various reaction steps were occurring over the entire temperature range examined, the maximum peak temperature was determined as 311.2 °C at 5 °C/min heating rate. The increase in the heating rate led to a shift in maximum peak temperature towards higher value due to the thermal lag. This value was 327.5 and 345.2 °C for 10 and 20 °C/min heating rate. Furthermore, the variation in heating rate affected the completion of the decomposition process. This process completed higher temperature with an incremental rise of the heating rate.

3.2. Kinetic Modelling

The thermal decomposition kinetics of the chitosan could be estimated on a single reaction and can be expressed under isothermal conditions by the following equation:

$$\frac{dx}{dt} = k(T)\,f(x) = A\exp\left(-\frac{E}{RT}\right) f(x) \quad (1)$$

where t is the time, x depicts the conversion degree, or extent of reaction, dx/dt is the isothermal reaction rate, and $f(x)$ is the conversion function that shows the reaction model used and depends on the controlling mechanisms. The extent of reaction, x, can be defined either as the mass fraction of chitosan that has decomposed as shown below:

$$x = \frac{w_0 - w_t}{w_0 - w_f} \quad (2)$$

where w_0 is the initial mass, w_t is the sample mass present at any time t, w_f is the final mass of sample. The non-isothermal rate expressions as a function of temperature at a linear heating rate, β, can be expressed in Equation 3.

$$\frac{dx}{dT} = \frac{dx}{dt}\frac{dt}{dT} \quad (3)$$

where dt/dT is the inverse of the heating rate, $1/\beta$, dx/dt shows the isothermal reaction rate, and dx/dT is the non-isothermal reaction rate. Thus, an expression of the rate law for non-isothermal conditions can be obtained by substituting Equation (3) into Equation (1):

$$\frac{dx}{dT} = \frac{k(T)\,f(x)}{\beta} = \frac{A}{\beta}\exp(-\frac{E}{RT})f(x) \quad (4)$$

Equation (4) could be integrated in Equation (5)

$$\int_0^x \frac{dx}{f(x)} = g(x) = \frac{A}{\beta}\int_{T_0}^{T}\exp(-\frac{E}{RT})dT = \frac{AE}{\beta R}\,p(u) \quad (5)$$

where $p(u)$ and $g(x)$ indicate the temperature integral and the integral form of the reaction model, respectively. Relied on the kinetic methods applied, $p(u)$ can be given by many linear approximations. To determine the chitosan kinetics, isoconversional methods can be used without reaction model estimation, $f(x)$. In this method, the value of the activation energy can be calculated at progressive degrees of conversion. Four isoconversional models for calculating activation energy from TG data are used in this study and these models were applied to main decomposition region (Akahira and Sunose, 1971; Starink 1966; Ozawa 1965; Nicolescu et al. 2015). The linear equations of each model are shown in Table 1.

Table 1. Linear equations of FWO, KAS, Starink, and Tang models

Kinetic model	General model equations
FWO	$\ln(\beta) = \ln\left(\frac{AE}{Rg(x)}\right) - 5.331 - 1.052\frac{E}{R}\frac{1}{T}$
KAS	$\ln\left(\frac{\beta}{T^2}\right) = \ln\left(\frac{AR}{Eg(x)}\right) - \frac{E}{RT}$
Starink	$\ln\left(\frac{\beta}{T^{1.92}}\right) = C - 1.0008\frac{E}{RT}$
Tang	$\ln\left(\frac{\beta}{T^{1.8947}}\right) = C - 1.0015\frac{E}{RT}$

By using the slopes of the plots obtained by linear equations of FWO, KAS, Starink, and Tang models, activation energy, the minimum energy requirement for a reaction started, can be calculated for each conversion degree. The typical plots for FWO, KAS, Starink, and Tang models are presented in Figure 2, respectively. As shown in Figure 2, the lines parallel each other and the similar parallelism trend was observed for all studied kinetic models. The parallelism of lines was attributed to the similar kinetic behavior and probably the single reaction mechanism was achieved.

Figure 3 and Table 2 show the activation energy value as a function of conversion degree for different kinetic models. It can be seen that the calculated average activation energy values were close to each other. The average activation energy value was calculated as 148.5, 146.4, 148.3 and 146.7 kJ/mol for FWO, KAS, Starink, and Tang models, respectively. The minor differences in calculated values were attributed to the solution of the integral function by using different approaches. The values for average activation energy calculated using different isoconversional methods were consistent with the previous study found in the literature (Moussout et al. 2016).

As can be seen in Table 2, the high R^2 (>0.98) values were obtained for the studied models. The good correlation coefficient indicated that the calculated activation energy values as a function of conversion degree in the range from 0.1 to 0.9 corresponding model data fitted the experimental data very well. That is, the results obtained were accurate and reliable.

To detect the appropriate reaction models for the thermal decomposition of the chitosan, fifteen different reaction models proposed by the Coats-Redfern method that considered the rate-limiting steps of diffusion, reaction or nucleation were utilized in this study (Ebrahimzad et al. 2017). The reaction mechanism and plotting methods are shown in Table 3.

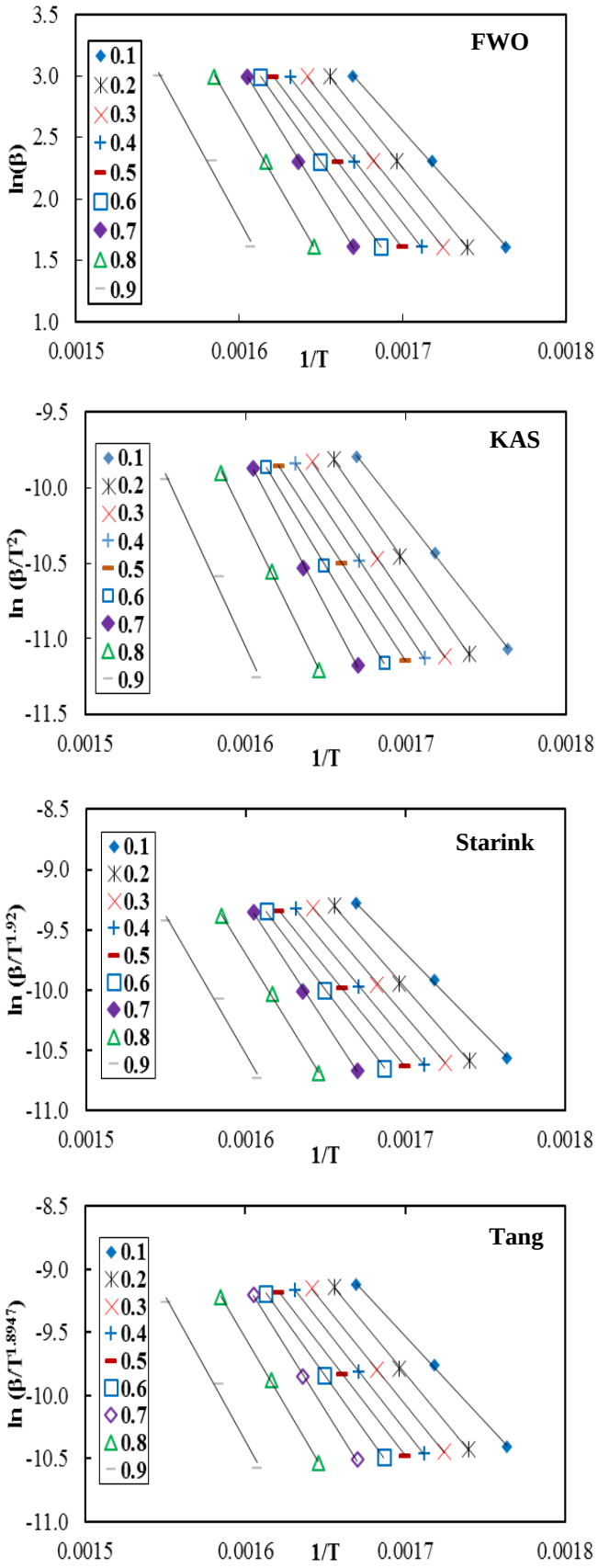

Figure 2. Plots for FWO, KAS, Starink, and Tang models

Table 2. The activation energy value according to conversion degree for FWO, KAS, Starink, and Tang models

x	FWO		KAS		Starink		Tang	
	E	R^2	E	R^2	E	R^2	E	R^2
0.1	112.1	0.9972	112.8	0.9990	125.0	0.9990	108.7	0.9993
0.2	129.6	0.9996	126.7	0.9997	126.9	0.9997	127.2	0.9990
0.3	132.4	0.9999	129.5	0.9999	129.8	0.9999	130.0	0.9994
0.4	135.9	0.9984	133.1	0.9999	133.4	0.9995	133.7	0.9988
0.5	138.5	0.9999	133.1	0.9992	136.0	0.9999	136.2	0.9989
0.6	148.3	0.9999	146.0	0.9991	146.2	0.9996	146.5	0.9991
0.7	168.6	0.9992	167.2	0.9998	167.4	0.9992	167.7	0.9991
0.8	180.0	0.9994	179.1	0.9993	179.4	0.9993	180.2	0.9990
0.9	190.4	0.9903	190.0	0.9891	190.3	0.9892	190.6	0.9988
Average	148.5		146.4		148.3		146.7	

The plots for various diffusion, nucleation, reaction order and geometric contraction models for 10 °C/min are given in Figure 4. The reaction mechanism applications were numbered according to the Table 3. The linear fitting was not obtained for diffusion controlled and nucleation reaction models.

The correlation coefficients, R^2, which are the criteria of how much the calculated model values and TG values match, are presented in Table 4. After examining the Table 4, it can be concluded that the reaction order model was the best model to statistically characterize the TG data and the highest R^2 values were provided for the second reaction order for all studied heating rates.

Table 3. Kinetic integration functions g(x) for different reaction mechanisms

No	Reaction mechanism	g(x)
Diffusion models		
1	One-dimensional diffusion	x^2
2	Two-dimensional diffusion (Valensi)	$x+[(1-x)\ln(1-x)]$
3	Three-dimensional diffusion (Jander)	$[1-(1-x)^{1/3}]^2$
4	Anti-Jander equation	$[(1+x)^{1/3}-1]^2$
5	Three-dimensional diffusion (Ginstling-Brounstein)	$1-(2/3)x-(1-x)^{2/3}$
Nucleation models		
6	Power law	x
7	Power law	$x^{1/2}$
8	Power law	$x^{1/3}$
9-11	n= 2, 3, 4 (Avrami-Erofeev)	$[-\ln(1-x)]^{1/n}$
Reaction order and geometric contraction models		
12	First-order (Mampel)	$-\ln(1-x)$
13	Reaction order (n=2)	$[(1-x)^{(1-n)}-1]/(n-1)$
14	Contraction of cylinder	$1-(1-x)^{1/2}$
15	Contraction of sphere	$1-(1-x)^{1/3}$

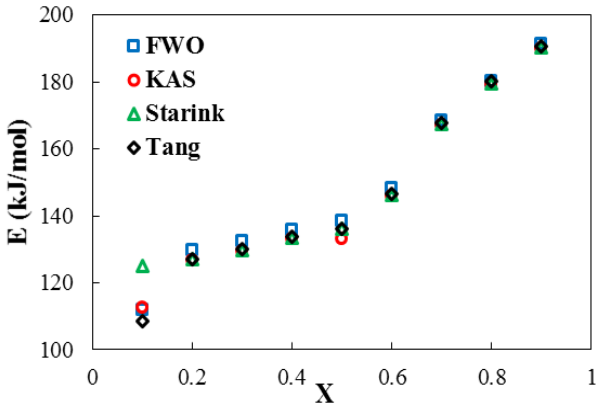

Figure 3. Calculated activation energy value with respect to conversion degree

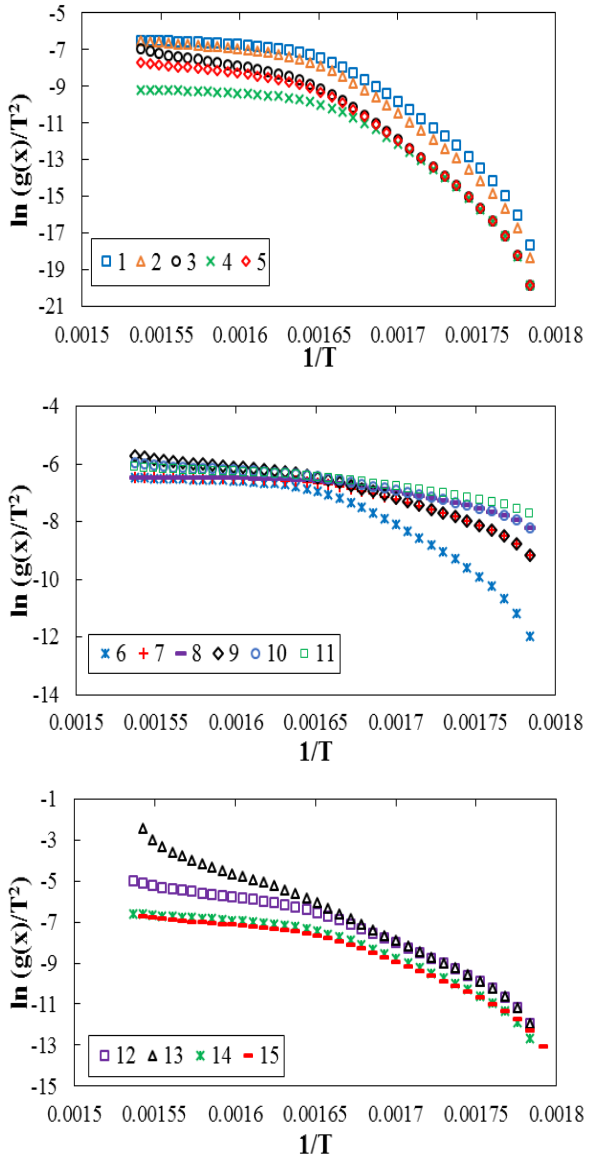

Figure 4. Variation models of chitosan for 10 °C/min heating rate

4. Conclusions

In this study, thermal decomposition experiments of chitosan were conducted in an inert N_2 atmosphere by means of a thermogravimetric analyzer. With the obtained TGA data, kinetic analysis was carried out, besides thermal behaviors of chitosan at different heating rates were investigated. FWO, KAS, Starink, and Tang kinetic models were utilized to calculate the activation energy. The average activation values were determined as 148.5, 146.4, 148.3 and 146.7 kJ/mol for FWO, KAS, Starink and Tang models, respectively. All models used provided accurate fits of each other with high R^2 values. In addition, it was determined that the second reaction order model was the best one to characterize the results among the other studied models.

Table 4. R^2 values for different reaction mechanisms

No	5 °C/min	10 °C/min	20°C/min
Diffusion controlled models			
1	0.8026	0.8321	0.8382
2	0.8337	0.8599	0.8651
3	0.8758	0.8968	0.9007
4	0.7821	0.8143	0.8209
5	0.8482	0.8727	0.8775
Nucleation reaction models			
6	0.7793	0.8274	0.8214
7	0.7202	0.8175	0.7800
8	0.6390	0.8068	0.7246
9	0.8836	0.9246	0.9123
10	0.8542	0.9208	0.8938
11	0.8132	0.9167	0.8694
Reaction order and geometric contraction models			
12	0.9053	0.9281	0.9264
13	**0.9814**	**0.9879**	**0.9955**
14	0.8471	0.8768	0.8622
15	0.8692	0.9032	0.8902

References

Akahira T, Sunose T 1971. Method of determining activation deterioration constant of electrical insulating materials. Res. Rep. Chiba Inst. Technol (Sci Technol) 16: 22-31.

Ebrahimzad H, Khayati GR, Schaffie M 2017. Preparation and kinetic modeling of β-$Co(OH)_2$ nanoplates thermal decomposition obtained from spent Li-ion batteries. Adv Powder Technol 28: 2779-2786.

Flynn JH, Wall LA 1966. General treatment of the thermogravimetry of polymers. J. Res. Nat. Bur. Stand 70: 487-523.

Hamedi H, Moradi S, Hudson SM, Tonelli AE 2018 Chitosan based hydrogels and their applications for drug delivery in wound dressings: A review. Carbohydrate Polymers 199: 445-460.

Kast CE, Valenta C, Leopold M, Bernkop-Schnürch A 2002. Design and in vitro evaluation of a novel bioadhesive vaginal drug delivery system for clotrimazole. Journal of Controlled Release 81: 347-354.

Lozano-Navarro JI, Díaz-Zavala NP, Velasco-Santos C, Melo-Banda JA, Páramo-García U, Paraguay-Delgado F, García-Alamilla R, Martínez-Hernández AL, Zapién-Castillo S 2018 Chitosan-Starch Films with Natural Extracts: Physical, Chemical, Morphological and Thermal Properties. Materials 11: 120.

Moussout H, Ahlafi H, Aazza M, Bourakhouadar M 2016. Kinetics and mechanism of the thermal degradation of biopolymers chitin and chitosan using thermogravimetric analysis. Polymer Degradation and Stability 130: 1-9.

Moussout H, Ahlafi H, Aazza M, Bourakhouadar M, Amechrouq A 2018. Bentonite/chitosan nanocomposite: Preparation, characterization and kinetic study of its thermal degradation. Thermochimica Acta 659: 191-202.

Nicolescu LC, Tita B, Jurca T, Marian E, Tita D 2015. Thermal Stability of Piroxicam – Active Substance and Tablets. I. Kinetic study of the active substance under nonisothermal conditions. Rev. Chim.-Bucharest 66: 1802-1806.

Ozawa T 1965. A new method of analyzing thermogravimetric data. Bulletin Chem. Soc. Japan 38: 1881-1886.

Starink M 1966. A new method for the derivation of activation energies from experiments performed at constant heating rate. Thermochimica Acta 288: 97-104.

Qu X, Wirsen A, Albertsson C 2000. Effect of lactic/glycolic acid side chains on the thermal degradation kinetics of chitosan derivatives. Polymer 41: 4841-4847.

Zhou L, Wang Y, Liu Z, Huang Q 2009. Characteristics of equilibrium, kinetics studies for adsorption of Hg(II), Cu(II), and Ni(II) ions by thiourea-modified magnetic chitosan microspheres. Journal of Hazardous Materials 161: 995-1002.

Eurasian J. Bio. Chem. Sci. 1(2): 48-53, 2018

EJBCS

Eurasian Journal of Biological and Chemical Sciences

Journal homepage: www.dergipark.gov.tr/ejbcs

Anti-cytotoxic-genotoxic influences of *in vitro* propagated *Bacopa monnieri* L. Pennell in cultured human lymphocytes

Muhammet Dogan*, Bugrahan Emsen

Department of Biology, Kamil Özdağ Faculty of Science, Karamanoğlu Mehmetbey University, Karaman, Turkey

*Corresponding author: mtdogan1@gmail.com
Orcid No: 0000 0003 3138 5903

Abstract: *Bacopa monnieri* L. Pennell is an important medicinal plant with antioxidant and neuroprotective role. It acts as an efficient free radical scavenger and has the potential to serve as a phytoremedy in the disease conditions involving reactive oxygen species (ROS) and oxidative stress. In addition, the protective role of *B. monnieri* on tissue antioxidant defense system and lipid peroxidative status in diabetic rats has been reported. *B. monnneri* used in the experiment was propagated by plant tissue culture techniques. The shoot tip explants of *B. monnneri* were cultured in Murashige and Skoog (MS) nutrient medium containing 1.0 mg/L 6-Benzylaminopurine (BAP). Genotoxic effects of aqueous extract obtained from *B. monnieri* in cultured human lymphocytes were determined by chromosome aberration (CA) test. In addition, cytotoxic activities of the extract on the cells were revealed via 3-(4,5-dimethylthiazol-2-yl)-2,5-diphenyltetrazolium bromide (MTT) analysis. Different concentrations (6.25-200 mg/L) of the extract were used in the treatments. It was detected that cytotoxicty was correlated with concentration. Cell viability decreased to 69.64% in the lymphocytes exposed to maximum concentration of the extract. Based on CA/cell test, the results were statistically ($p > 0.05$) indifferent from negative control treatment. Overall, obtained data indicated that *B. monnieri* is a plant that contains natural products that are not causative of cytotoxic and genotoxic damage on human lymphocytes.

Keywords: Cytotoxicity, Genotoxicity, Shoot Regeneration

1. Introduction

The immune system protects the body from microorganisms, cancer cells, fungi, toxins, chemicals and foreign substances. This important system recognizes molecules called antigens and neutralizes them by means of antibodies or immunoglobulins of different structure (Zumla and James, 2002; Łukasiewicz and Fol, 2018). The cells involved in the immune system are leukocytes. Leukocytes produced in various organs such as spleen, bone marrow, thymus and lymph nodes are effective on antigens. Lymphocytes, a variety of leukocytes, are the most important elements of the acquired immune system (Feng et al., 2016; Imai et al., 2017). Lymphocytes are produced to create defenses against diseases. Lymphocytes rise in some cases. This usually means that the metabolism stimulates the immune system against a disease and the lymphocyte count increases (Valdez et al., 2002; Kazmin et al., 2005). Lymphocyte deficiency is seen when the immune system can not produce enough lymphocyte cells (Mäurer et al., 2002; Wiesner et al., 2017).

The antioxidants in our body stimulate the lymphocyte proliferation and ensure that the immune system remains active. In this way, oxidative and genetic damage rates that cause many diseases will decrease (Rodríguez-Ribera et al., 2016; Jafarpour et al., 2018; Sevindik et al., 2018). Genetic damage that occurs in cells is transferred to future generations and permanent diseases can take place (Lin et al., 2018). In particular, damage to cells such as lymphocytes breaks the body's resistance (Ruehl-Fehlert et al., 2017).

In the treatment processes, it is of great importance that the side effects of the drugs taken on the body are low and do not cause serious problems such as genetic damage (Luu and Palczewski, 2018). The chemical properties of herbal products, which are frequently preferred recently, should be examined in detail. It should be determined that plant products do not adversely affect healthy cell proliferation and do not cause genetic damage (Gadano et al., 2006; Emsen et al., 2017). This is usually due to the antioxidant capacity of these natural products (Karatas et al., 2015; Sevindik et al., 2017; Emsen and Dogan, 2018).

Bacopa monnieri (L.) Pennell (Scorphulariaceae), commonly known as Brahmi (Sharma et al., 2010), grows in wetlands such as pools, streams and lakeside edges. *B. monnieri* has spread in India, Pakistan, Afghanistan, Nepal, Sri Lanka, subtropical USA, tropical Asia, Africa

and Australia (Russo and Borrelli, 2005). It has long been used in the traditional Ayurvedic medicine system to improve intelligence and memory (Uabundit et al., 2010). In an experiment conducted on seventy-six adults aged 40 and 65 years, *B.monnieri* showed a significant effect on retention of new information and memory enhancement (Roodenrys et al., 2002). It is known in the traditional medical system that *B. monnieri* is used as nerve tonic, diuretic, cardiotonic and therapeutic agents against epicopsies, insomnia, asthma and rheumatism. Many studies have shown that this plant extract has anxiolytic, anti-depression and antioxidant activity (Bhattacharya et al., 2000; Uabundit et al., 2010). *B. monnieri* has been reported to have antiinflammatory, analgesic, antipyretic, sedative, free radical scavenging and anti-lipid peroxidative activity (Mathew et al., 2010). The plant is astringent, bitter, sweet, cooling, laxative, intellect promoting, anodyne, carminative, digestive, antiinflammatory, anticonvulsant, depurative, cardiotonic, bronchodialator, diuretic, emmenagogue, sudorfic, febrifuge and tonic (Rastogi et al., 1994; Mathew et al., 2010).

To the best of our knowledge the effects of *in vitro* propagated *B. monnieri* in cultured human lymphocytes (HLs) were not investigated. Therefore, in this investigation, it was aimed to describe the cyto-genotoxic influences of aqueous extract obtained from *B. monnieri* on HLs. With this aim, 3-(4,5-dimethylthiazol-2-yl)-2,5-diphenyltetrazolium bromide (MTT), mitotic index (MI) and chromosome aberration (CA) analyses were performed on HLs exposed to the aqueous extract of *B. monnieri*.

2. Materials and Method

2.1. In vitro plant propagation

Sterilized *B. monnieri* plants were obtained from the Biology Department of Karamanoğlu Mehmetbey University. The shoot tip explants of *B. monnieri* were cultured in MS (Murashige and Skoog, 1962) nutrient medium (Table 1) supplemented with 1.0 mg/L 6-Benzylaminopurine (BAP) at 24°C for 16 hours in light and 8 hours in dark photoperiod. MS medium and vitamins, 3% sucrose and 0.65% agar were used in all culture media. Distilled water was used for the preparation of the nurient medium. The pH of the nutrient medium was adjusted to 5.7±1 using 1N NaOH and 1N HCl, followed by sterilization at 1.2 atmospheres pressure and at 120°C for 20 minutes. In the experiments, the explants were incubated under a white LED (Light-Emitting Diode) light (1500 lux) at a temperature of 24°C and a 16 hour light photoperiod for ten weeks. Experiments were carried out in magenta containers in 3 replicates.

2.2. Extraction of bioactive ingredients

Entire samples of *B. monnieri* were used for extraction. Fine dried powdered samples were prepared using liquid nitrogen, mortar and pestle from 10 g of whole samples. The extracts were obtained in 250 mL of distilled water using Soxhlet extraction apparatus for two days. Thereafter, the solvent were evaporated using rotary evaporator under vacuum to dryness and extract with 6.25, 12.5, 25, 50, 100 and 200 mg/mL concentration were prepared. The yields were based on dry materials of plant sample. The analyses tested without extract formed the negative control (Control (-)) group.

Table 1. The content of Murashige and Skoog (1962) basic nutrient medium

Components		Concentrations (mg/L)
Macroelements	NH_4NO_3	1650.000
	KNO_3	1900.000
	$CaCI_2.2H_2O$	440.000
	$MgSO_4.7H_2O$	370.000
	KH_2PO_4	170.000
Microelements	KI	0.830
	H_3BO_3	6.200
	$MnSO_4.4H_2O$	22.300
	$ZnSO_4.7H_2O$	8.600
	$Na_2MoO_4.2H_2O$	0.250
	$FeSO_4.7H_2O$	27.850
	$CoCl_2.6H_2O$	0.025
	$CuSO_4.5H_2O$	0.025
	$Na_2EDTA.2H_2O$	37.250
Vitamins	Myo-Inositol	100.000
	Nicotinic Acid	0.500
	Pyrotinic Acid	0.500
	Thiamine-HCI	0.100
	Glycine	2.000

2.3. HLs culture

HLs in the heparinized blood samples were separated by density gradient using Ficoll-Hypaque (Sigma Aldrich, St Louis, MO, USA). Later, isolated HLs were incubated in RPMI-1640 medium (Sigma-Aldrich, St Louis, MO, USA) with 2 mM/L L-glutamine, 10% FBS, and penicillin-streptomycin (Sigma-Aldrich, St Louis, MO, USA) in the presence of 5% CO_2 at 37°C at 1×10^6 cells/mL.

2.4. MTT assay

The cells were seeded in 96-well plates. Cells were incubated at 37°C in a humidified 5% CO_2/95% air mixture and treated with extracts at different concentrations (6.25, 12.5, 25, 50, 100 and 200 mg/mL) for 24 h. The MTT assay was carried out using a commercially available kit (Cayman Chemical Company, Ann Arbor, MI, USA). In MTT assays, mitomycin-C ($C_{15}H_{18}O_5$, Sigma, St Louis, MO, USA, at 10^{-7} M) chemotherapeutic agent was used as a positive control (Control (+)).

2.5. CA assay

Heparinized blood was cultured in 6 mL of culture medium (Chromosome Medium B; Biochrom, Berlin) with

5 mg/mL of phytohemagglutinin (Biochrom, Berlin). The cultures were incubated in complete darkness for 72 h at 37ºC. Two hours prior to harvesting, colchicine (Sigma-Aldrich, St Louis, MO, USA) at a final concentration of 2 mg/mL was added to the culture flask. Hypotonic treatment and fixation were performed. To prepare slides, 3-5 drops of the fixed cell suspension were dropped on a clean slide and air-dried. The slides were stained in 3% Giemsa solution in phosphate buffer (pH 6.8) for 15 min. For each treatment, 30 well-spread metaphases were analyzed to detect the presence of chromosomal aberrations. In CA assay, it was used mitomycin-C ($C_{15}H_{18}N_4O_5$, Sigma, St, Louis/MO, USA, at 10^{-7} M) as control (+). MI was also calculated based on number of cells in metaphase.

2.6. Statistical analyses

Mean values of different activities of the extracts were compared with analysis of variance by Duncan's multiple range test for comparing groups. A significance level of 5% was accepted for all comparisons. Median inhibitory concentration (IC_{50}) values were calculated with probit regression analysis and associated 95% confidence limits for each treatment. Pearson's correlation coefficients were used in order to determine relation levels among the variables. These calculations were carried out using the Statistical Package for Social Sciences (SPSS, version 21.0, IBM Corporation, Armonk, NY, USA).

3. Results and Discussion

Tissue culture techniques are one of the most effective techniques for propagation of plants. The production of many medicinal plants with tissue culture such as *Hypericum rumeliacum* Boiss (Danova et al., 2010), *Alternanthera sessilis* (L.) (Gnanaraj et al., 2011), *Harpagophytum procumbens* (Bairu et al., 2011), *Aloe arborescens* Mill (Amoo et al., 2012), *Coleonema pulchellum* (Baskaran et al., 2014), *Ceratophyllum demersum* L. (Dogan et al., 2015), *Rotala rotundifolia* (Buch-Ham. ex Roxb) Koehne (Dogan, 2017) *Lysimachia nummularia* L. (Dogan, 2018a), *Limnophila aromatica* (Lamk.) Merr. (Dogan, 2018b), *Actinidia melanandra* Franch. and *Actinidia rubricaulis* Dunn. (Bourrain, 2018) has been previously reported.

In this study, the shoot tip explants of *B. monnieri* for rapid and multiple production were cultured in MS medium containing 1.0 mg/L BAP for 10 weeks. Regenerated shoots on explants within two weeks have started to appear. At the end of four weeks, multiple shoot formations were clearly observed in the culture medium. High shoot regeneration frequency was obtained in all culture media. The rapid and multiple production of *B. monnieri* has been achieved successfully after 10 weeks of culture (Figure 1). Similarly, *in vitro* propagation of *B. monnieri* in previous studies have been reported (Showkat et al., 2010; Vijaykumar et al., 2010; Shrivastava et al., 2017; Naik et al., 2017; Kashyap et al., 2018).

Cytotoxic effects of different concentrations of the extract on HLs were assessed by MTT and MI tests. Results exhibited a concentration-dependent increase in growth inhibition of HLs. Cell viability percentages of HLs exposed to maximum concentrations of the extract were 69.64% (Figure 2a). In another study performed on HLs, similar results were obtained as regarding concentration dependent cytotoxicity. It was reported that olivetoric and physodic acid isolated from *Pseudevernia furfuracea* (L.) Zopf lichen decreased viability of HLs depending on the concentration (Emsen et al., 2018c). In the aforementioned study, it was detected that cytotoxicity was stable the treatments with high concentrations. At the same time, calculated MI values indicated that the treatments with high concentration were more effective on the cells. The lowest concentration (6.25 mg/L) of the extract did not significantly ($p > 0.05$) increase MI value (5.25%) in the cells compared with control (-). It was reflected in the results that cell proliferation did not change significantly in low concentration trials (Figure 2b). The cytotoxic effects of different plant species on HLs was tested by the researchers (Gadano et al., 2006). It was suggested that aqueous extracts obtained from *Chenopodium ambrosioides* L. and *C. multifidum* L. caused decreasing in MI in the cells. In a different MI-natural product study, an insignificant decrease in the MI rate in HLs was determined (Ari et al., 2015). In this study, *Parmelia sulcata* lichen extract was used and a significant difference was found between the control (+) and the extract trial results. In the present study, the values in the cells exposed to control (+) were significantly ($p < 0.05$) different from all other trial results for both MTT and MI activities.

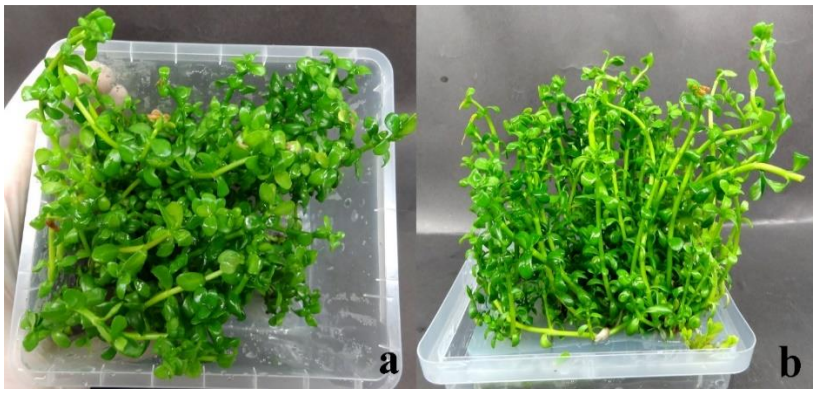

Figure 1. *In vitro* plant regeneration from shoot tip explants of *B. monnieri* (a,b) after 10 weeks of culture

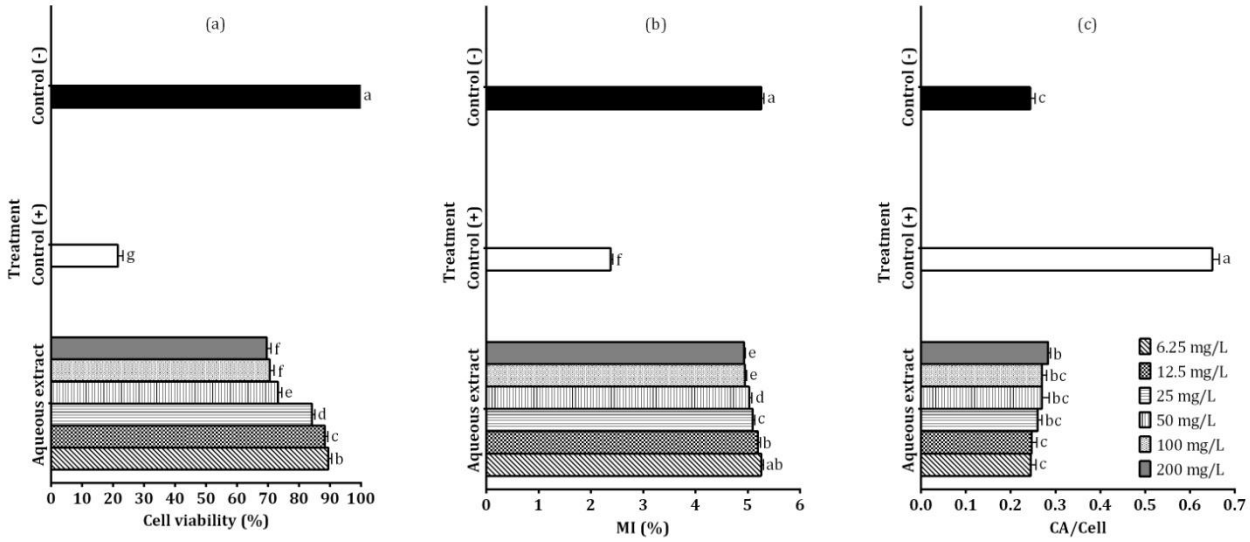

Figure 2. (a) Viability rate, (b) MI percentage and (c) CA frequency in the HPLs exposed to aqueous extract from *B. monnieri*. Different small letters indicate significant differences among treatments at $p < 0.05$.

Table 2. IC_{50} value for HLs exposed to aqueous extract from *B. monnieri* (mg/L)

IC_{50} (limits)	Slope ± standard error (limits)	X^2
1129.45 (579.92-3224.04)	0.56 ± 0.07 (0.43-0.69)	7.05

Table 3. Correlation between different variables for HLs exposed to aqueous extract from *B. monnieri*

	CA	Cell viability	Concentration	MI
CA	1[a]			
Cell viability	-0.73**	1		
Concentration	0.69**	-0.81**	1	
MI	-0.68**	0.95**	-0.82**	1

[a]Pearson correlation coefficient; **correlation is significant at the 0.01 level

Based on the experiments with high concentrations of the extracts, it was determined that there was no statistically ($p > 0.05$) significant difference between concentrations of 100 and 200 mg/L of the extracts in both MTT and MI activities. Additionally, IC_{50} value of the extract found to be 1129.45 mg/L indicated that very high concentrations of aqueous extract obtained from *B. monnieri* showed cytotoxic effect on the cells (Table 2). In another study carried out with plant-based products, it was used copaene, a tricyclic sesquiterpene. According the MTT results of previous mentioned study, copaene significantly suppressed the proliferation of HLs at high concentrations (Turkez et al., 2014). Similar relationship was found in the study performed with ascorbic acid, a strong antioxidant compound. Low proliferation index in titanium dioxide-induced HLs was increased by ascorbic acid treatment (Turkez, 2011).

Genetic damage emerged in HLs by aqueous extract obtained from *B. monnieri* was measured with CA analysis occurring in the cells. It was observed that the extracts increased CA frequency in HLs in a dose-dependent manner. However, there was no statistically ($p > 0.05$) significant difference between CA rates caused by extract treatments and control (-) except for the highest concentration. The CA data in HLs exposed to the extracts were too far and significantly ($p < 0.05$) different from the control (+) value (0.65 CA/cell) (Figure 2c). Numerous studies were conducted to inhibit the genetic damage caused by different toxic substances in the lymphocytes with natural products. Resveratrol (Turkez and Aydin, 2013), boron (Geyikoglu and Turkez, 2008), propolis (Bayram et al., 2016) and boric acid (Turkez et al., 2010) are some of these natural products. In the literature, studies on antigenotoxic activity carried out with different organism species such as *Bryoria capillaris* (Ach.) Brodo & D. Hawksw, *Xanthoria elegans* (Link) Th. Fr. (Aydin and Turkez, 2011a), *Aspicilia calcerea* (L.) Körb., *Cetraria chlorophylla* (Willd.) Poetsch (Aydin and Turkez, 2011b), *Platismatia glauca* (L.) W.L. Culb. & C.F. Culb. (Emsen et al., 2018a) and *Cladonia furcata* (Huds.) Schrad. (Emsen et al., 2018b) on HLs are also available.

When different activities of the extracts in HLs are examined, relationship between the activities was noteworthy. Bivariate correlation analysis performed on the data indicated that there were significantly ($p < 0.01$) negative correlations between several binary variables (cell viability-CA, cell viability-concentration, MI-CA and MI-concentration). In addition, concentration-CA and MI-cell viability bivariate correlations for the extract experiments were significant at the 0.01 level (Table 3).

5. Conclusions

In conclusion, we have displayed that aqueous extract obtained from *B. monnieri*, which is an important medicinal plant, does not show cytotoxic and genotoxic effects on cultured HLs especially in 6.25-50 mg/L concentration applications. So, this plant can be a new resource of therapeutics as recognized in this study against genetic damages. At the same time, thanks to the multiple production of the plant under *in vitro*, the plant will not need to be collected from its natural environment and the problem of being attached to the external environment and disrupting the balance in the ecosystem may be eliminated.

References

Amoo SO, Aremu AO, Staden JV 2012. *In vitro* plant regeneration, secondary metabolite production and antioxidant activity of micropropagated *Aloe arborescens* Mill. Plant Cell Tissue Organ Cult 111: 345-358.

Ari F, Ulukaya E, Oran S, Celikler S, Ozturk S, Ozel MZ 2015. Promising anticancer activity of a lichen, *Parmelia sulcata* Taylor, against breast cancer cell lines and genotoxic effect on human lymphocytes. Cytotechnology 67: 531–543.

Aydin E, Turkez H 2011a. Effects of lichenic extracts (*Bryoria capillaris*, *Peltigera rufescens* and *Xanthoria elegans*) on human blood cells: A cytogenetic and biochemical study. Fresenius Environ Bull 20: 2992–2998.

Aydin E, Turkez H 2011b. Antioxidant and genotoxicity screening of aqueous extracts of four lichens collected from North East Anatolia. Fresenius Environ Bull 20: 2085–2091.

Bairu MW, Amoo SO, Staden JV 2011. Comparative phytochemical analysis of wild and *in vitro*-derived greenhouse-grown tubers, *in vitro* shoots and callus-like basal tissues of *Harpagophytum procumbens*. S Afr J Bot 77: 479-484.

Baskaran P, Moyo M, Staden JV 2014. *In vitro* plant regeneration, phenolic compound production and pharmacological activities of *Coleonema pulchellum*. S Afr J Bot 90: 74-79.

Bayram S, Ecem Bayram N, Gerçek YC, Öz GC, Sorkun K 2016. Anticytotoxic and antimutagenic effects of propolis on human lymphocytes *in vitro*. Mellifera 16: 38–46.

Bhattacharya SK, Bhattacharya A, Kumar A, Ghosal S 2000. Antioxidant activity of *Bacopa monnieri* in rat frontal cortex, striatum and hippocampus. Phytother Res 14: 174-179.

Bourrain L 2018. *In vitro* propagation of *Actinidia melanandra* Franch. and *Actinidia rubricaulis* Dunn. from shoot tip explants. N Z J Crop Hortic Sci 46(2): 162-173.

Danova K, Cellárová E, Macková A, Daxnerová Z, Kapchina-Toteva V 2010. *In vitro* culture of *Hypericum rumeliacum* Boiss and production of phenolics and flavonoids. *In Vitro* Cell Dev Biol 46: 422-429.

Dogan M, Karatas M, Aasim M 2015. An efficient *in vitro* plantlet regeneration of *Ceratophyllum demersum* L., an important medicinal aquatic plant. Fresen Environ Bull 24(10b): 3499-3504.

Dogan M 2017. Multiple shoot regeneration from shoot tip and nodal explants of *Rotala rotundifolia* (Buch-Ham. ex Roxb) Koehne. Ant J Bot 1(1,2): 4-8.

Dogan M 2018a. Tıbbi bitki *Lysimachia nummularia* L.'nın boğum eksplantlarından *in vitro* mikroçoğaltımı. KSÜ Tarım ve Doğa Dergisi, 21(6): 875-881.

Dogan M 2018b. *Limnophila aromatica* (Lamk.) Merr.'nın boğum ve boğum arası eksplantlarından *in vitro* sürgün rejenerasyonu. Iğdır Üniversitesi Fen Bilimleri Enstitüsü Dergisi 8(3): 77-84.

Emsen B, Turkez H, Togar B, Aslan A 2017. Evaluation of antioxidant and cytotoxic effects of olivetoric and physodic acid in cultured human amnion fibroblasts. Hum Exp Toxicol 36: 376–385.

Emsen B, Dogan M 2018. Evaluation of antioxidant activity of *in vitro* propagated medicinal *Ceratophyllum demersum* L. extracts. Acta Sci Pol Cultus 17: 23–33.

Emsen B, Aslan A, Kaya A 2018a. Biological activities of *Platismatia glauca* (L.) W.L.Culb. & C.F.Culb. on human lymphocytes. Süleyman Demirel Univ J Nat Appl Sci 22: 840–848.

Emsen B, Aslan A, Kaya A 2018b. Cytotoxic, genotoxic and oxidative effects of *Cladonia furcata* (Huds.) Schrad. on human peripheral lymphocytes. Cumhur Sci J 39: 169–180.

Emsen B, Togar B, Turkez H, Aslan A 2018c. Effects of two lichen acids isolated from *Pseudevernia furfuracea* (L.) Zopf in cultured human lymphocytes. Zeitschrift fur Naturforsch Sect C-A J Biosci 73: 303–312.

Feng L, Huang Q, Huang Z, Li H, Qi X, Wang Y, Liu Z, Liu X, Lu L 2016. Optimized animal model of cyclophosphamide-induced bone marrow suppression. Basic Clin Pharmacol Toxicol 119: 428–435.

Gadano AB, Gurni AA, Carballo MA 2006. Argentine folk medicine: genotoxic effects of Chenopodiaceae family. J Ethnopharmacol 103: 246–251.

Geyikoglu F, Turkez H 2008. Boron compounds reduce vanadium tetraoxide genotoxicity in human lymphocytes. Environ Toxicol Pharmacol 26: 342–347.

Gnanaraj WE, Marimuthu J, Subramanian KM, Nallyan S 2011. Micropropagation of *Alternanthera sessilis* (L.) using shoot tip and nodal segments. Iran J Biotechnol 9: 206-212.

Imai Y, Ishida K, Nemoto M, Nakata K, Kato T, Maéno M 2017. Multiple origins of embryonic and tadpole myeloid cells in *Xenopus laevis*. Cell Tissue Res 369: 341–352.

Jafarpour SM, Safaei M, Mohseni M, Salimian M, Aliasgharzadeh A, Fahood B 2018. The radioprotective effects of curcumin and trehalose against genetic damage caused by I-131. Indian J Nucl Med 33: 99–104.

Karatas M, Dogan M, Emsen B, Aasim M 2015. Determination of *in vitro* free radical scavenging activities of various extracts from *in vitro* propagated *Ceratophyllum demersum* L. Fresenius Environ Bull 24: 2946–2952.

Kashyap S, Kapoor N, Kale RD 2018. Micropropagation of B. monnieri using humin media in plant tissue culture. Ann Plant Sci 6(5): 1625-1629.

Kazmin SD, Todor IN, Chekhun VF 2005. Antitumor resistance activation in mice: Can the immunological memory cells enhance resistance? J Exp Clin Cancer Res 24: 585–593.

Lin X-F, Luo J-W, Gui LIU, Zhu Y-B, Zhao JIN, Xing LIN 2018. Genetic mutation of familial dilated cardiomyopathy based on next-generation semiconductor sequencing. Mol Med Rep 18: 4271–4280.

Łukasiewicz K, Fol M 2018. Microorganisms in the treatment of cancer: advantages and limitations. J Immunol Res 2018: 2397808.

Luu J, Palczewski K 2018. Human aging and disease: lessons from age-related macular degeneration. Proc Natl Acad Sci U S A 115: 2866–2872.

Mathew J, Paul J, Nandhu MS, Paulose CS, 2010. *Bacopa monnieri* and Bacoside-A for ameliorating epilepsy associated behavioral deficits. Fitoterapia 81: 315-322.

Mäurer M, Kobsar I, Berghoff M, Schmid CD, Carenini S, Martini R 2002. Role of immune cells in animal models for inherited neuropathies: facts and visions. J Anat 200: 405–414.

Murashige T, Skoog F 1962. A revised medium for rapid growth and bioassays with tobacco tissue cultures. Plant Physiol 15: 473-497.

Naik PM, Godbole M, Nagella P, Murthy HN 2017. Influence of different media, medium strength and carbon sources on adventitious shoot cultures and production of bacoside A in *Bacopa monnieri* (L.). Ceylon J Sci 46(4): 97-104.

Rastogi S, Pal R, Kulshreshtha DK 1994. Bacoside A3-a triterpenoid saponin from *Bacopa monniera*. Phytochemistry 36: 133-137.

Rodríguez-Ribera L, Pastor S, Corredor Z, Silva I, Diaz JM, Ballarin J, Marcos R, Coll E 2016. Genetic damage in patients moving from hemodialysis to online hemodiafiltration. Mutagenesis 31: 131–135.

Roodenrys S, Booth D, Bulzomi S, Phipps A, Micallef C, Smoker J 2002. Chronic effects of Brahmi (*Bacopa monnieri*) on human memory. Neuropsychopharmacology 27: 279-281.

Ruehl-Fehlert C, Parker GA, Elmore SA, Kuper CF 2017. Immune System. In: Fundamentals of Toxicologic Pathology: Third Edition. pp. 273–313.

Russo A, Borrelli F 2005. *Bacopa monniera*, a reputed nootropic plant: an overview. Phytomedicine 12: 305-317.

Sevindik M, Akgul H, Pehlivan M, Selamoglu Z 2017. Determination of therapeutic potential of *Mentha longifolia* ssp. *longifolia*. Fresen Environ Bull 26: 4757-4763.

Sevindik M, Akgul H, Dogan M, Akata I, Selamoglu Z 2018. Determination of antioxidant, antimicrobial, DNA protective activity and heavy metals content of *Laetiporus sulphureus*. Fresen Environ Bull 27(3): 1946-1952.

Sharma S, Kamal B, Rathi N, Chauhan S, Jadon V, Vats N, Gehlot A, Arya S 2010. *In vitro* rapid and mass multiplication of highly valuable medicinal plant *Bacopa monnieri* (L.) Wettst. Afr J Biotechnol 9(49): 8318-8322.

Showkat P, Zaidi Y, Asghar S, Jamaluddin S. 2010. *In vitro* propagation and callus formation of *Bacopa monnieri* (L.) Penn. Plant Tissue Cult & Biotech 20(2): 119-125.

Shrivastava P, Tiwari KN, Srivastava G 2017. Effect of different carbon sources on *in vitro* regeneration of Brahmi *Bacopa monnieri* (L.) An important memory vitalizer. J Med Plant Res 5(3): 202-208.

Turkez H, Tatar A, Hacimuftuoglu A, Ozdemir E 2010. Boric acid as a protector against paclitaxel genotoxicity. Acta Biochim Pol 57: 95–97.

Turkez H 2011. The role of ascorbic acid on titanium dioxide-induced genetic damage assessed by the comet assay and cytogenetic tests. Exp Toxicol Pathol 63: 453–457.

Turkez H, Aydin E 2013. The genoprotective activity of resveratrol on permethrin-induced genotoxic damage in cultured human lymphocytes. Brazilian Arch Biol Technol 56: 405–411.

Turkez H, Celik K, Togar B 2014. Effects of copaene, a tricyclic sesquiterpene, on human lymphocytes cells *in vitro*. Cytotechnology 66: 597–603.

Uabundit N, Wattanathorn J, Mucimapura S, Ingkaninan K 2010. Cognitive enhancement and neuroprotective effects of *Bacopa monnieri* in Alzheimer's disease model. J Ethnopharmacol 127(1): 26-31.

Valdez H, Connick E, Smith KY, Lederman MM, Bosch RJ, Kim RS, St. Clair M, Kuritzkes DR, Kessler H, Fox L, Blanchard-Vargas M, Landay A 2002. Limited immune restoration after 3 years' suppression of HIV-1 replication in patients with moderately advanced disease. AIDS 16: 1859–1866.

Vijaykumar M, Vijaykumar R, Stephen R 2010 *In vitro* propagation of *Bacopa monnieri* L.-A multipurpose medicinal plant. ndian J Sci Technol 3(7): 781-786.

Wiesner DL, Smith KD, Kashem SW, Bohjanen PR, Nielsen K 2017. Different lymphocyte populations direct dichotomous eosinophil or neutrophil responses to pulmonary cryptococcus infection. J Immunol 198: 1627–1637.

Zumla AI, James DG 2002. Immunologic aspects of tropical lung disease. Clin Chest Med 23: 283–308.

Eurasian J. Bio. Chem. Sci. 1(2): 54-58, 2018

EJBCS

Eurasian Journal of Biological and Chemical Sciences

Journal homepage: www.dergipark.gov.tr/ejbcs

Fabrication and characterization of PCL/ZnO-NP nanocomposite for wound dressing applications

Alev Akbaş [1]*, Melek Erol Taygun [1], Sadriye Küçükbayrak [1]

[1] *Istanbul Technical University, Chemical & Metallurgical Engineering Faculty, Chemical Engineering Department, İstanbul, Turkey*

*Corresponding author : akbas16@itu.edu.tr
Orcid No: 0000-0002-4092-8474

Abstract: Nanotechnology has a critical role in biotechnology and medicine with aiming to develop portable, low cost, safe and practical technologies. One of these technologies includes construction of three dimensional biomimetic nanofiber scaffolds with using electrospinning method. Nanofibers have started to be used with the development of nanotechnology in tissue engineering because of its similarity to natural human tissues. The architecture of original extracellular matrix at nanoscale level can be mimicked by these scaffolds. Meanwhile, metal nanoparticles are also used in tissue engineering because of their unique features such as optical, electronic, catalytic, and antibacterial. Zinc oxide (ZnO) is a transition metal oxide and it has good catalytic, electrical, photochemical, optical, antibacterial, enhanced cell proliferation and wound healing properties. Zn ion also acts as regulator for auto debridement and keratinocyte migration, both of which are essential for wound repair. Polycaprolactone (PCL) which is biocompatible and biodegradable synthetic polymer used as biomaterial for various biomedical applications such as tissue engineering scaffolds and wound dressings. In the present study, zinc oxide nanoparticles (ZnO-NPs) synthesized by microwave irradiation were used for the fabrication of PCL/ZnO-NP nanocomposite via electrospinning method. The effects of the ZnO nanoparticle concentration on the fiber diameter and fiber morphology were investigated using a scanning electron microscope (SEM). The presence of ZnO-NPs in the structure was determined by X-ray diffraction (XRD). It was observed that the average diameter of nanofibers was below micrometers. Overall results showed that PCL/ZnO-NP nanocomposite were found to be suitable for wound dressing applications.

Keywords: ZnO nanoparticle, PCL, nanofiber, microwave irradiation, wound dressing, antibacterial.

1. Introduction

Nanotechnology is an emerging field of science which deals with synthesis and development of materials at the scale of nanometer. Recent advancements in the field of nanotechnology opened new channels for its applications in biomedical area. Tissue engineering is one of the biomedical applications and is an interdisciplinary field to build biological substitutes that restore or improve the function of injured tissue (Liu et al., 2017). Tissue engineering is used to fabricate functional constructs, scaffolds, which are ranging from one dimension (1D) to three dimension (3D) structures. Scaffolds play an important role for the formation of the extracellular matrix (ECM) and restore damaged tissues via cell proliferation and migration (Augustine et al., 2014). Among the various scaffold fabrication techniques, electrospinning presents substantial advantages to be able to obtain uniform and continuous nanofibers and fabrics with adjustable pore structure and diameters ranging from nanometers to micrometers from synthetic (PCL, PGA, PLGA, PVA) and many natural (collagen, gelatin, chitosan, fibrin) polymers. The nanofibers with adjustable pore structure and large surface to volume ratio have been used in many fields particularly biomedical applications such as tissue scaffold, wound dressing and drug delivery (Liu et al., 2017).

Wound dressing materials act as physical barriers to maintain permeability for moisture and oxygen and to protect the wound mainly against microorganisms (Mogoşanu et al., 2014). A standard wound dressing material should be non-toxic and have good permeability as well as skin flexibility, biocompatibility and biodegradability characteristics. In contrast to traditional cotton-gauge dressings which do not adequately meet the requirements of wound care, fiber mats fabricated by electrospinning technique have potential to provide an excellent platform for wound healing. Nanofibers fabricated by electrospinning process have high surface area to volume ratio, high porosity and gas permeability. These properties provide to accelerate wound healing by increasing in the rate of gas permeability for cell, skin regeneration , moisture regeneration, removal of exudates and hemostasis (Rath et al., 2016). Wound dressings that are impregnated with antimicrobials (Ag nanoparticles (Wei et al., 2016), ZnO nanoparticles (ZnO NPs) (Augustine et al., 2014)), growth

factors, collagen or enzyme debriding agents can accelerate wound healing and show antimicrobial properties (Mogoşanu et al., 2014).

Zinc oxide (ZnO) is a unique material with a wide band gap of 3.37 eV and a large excitation binding energy (60 meV) (Faal Hamedani and Farzaneh, 2006). ZnO is currently listed as a 'generally recognized as safe' (GRAS) material by the Food and Drug Administration and is used as a food additive (Augustine et al., 2014). It is generally utilized in many dermatological applications including sunscreens, and skin care products and enhanced healing of wounds (Shoja et al., 2015). Zinc deficiency extends the healing period of wounds. ZnO NPs are one of the best appropriate source for wound applications by enhancing re-epithelialization, reducing inflammation and bacterial growth. Zinc being the cofactor of metaloprotein plays an important role in the regeneration of ECM. Moreover, Zinc also acts as regulator for auto debridement and keratinocyte migration, both of which are essential for wound repair (Landsdown et al., 2007). ZnO NPs can improve cell adhesion, proliferation and cell migration through growth factor mediated pathways by causing reactive oxygen species (ROS) production. (Augustine et al., 2014; Toduka et al., 2012; Premanathan et al., 2011). The ZnO NP can be synthesized by using various techniques such as hydrothermal, sol–gel, precipitation, microemulsion, chemical vapor deposition and solid state reaction (Król et al., 2017). The utilization of microwave irradiation as a heating method in the synthesizing of nanoparticles has the advantages of producing small particle size with high purity due to short reaction time compared to the conventional methods (Faal Hamedani and Farzaneh, 2006). PCL which is non-toxic, biocompatible, biodegradable and synthetic aliphatic polyester in biomedical applications can be used in drug delivery devices, tissue engineering scaffolds and wound dressings (Augustine et al., 2014; Shoja et al., 2015, Liu et al., 2017). In the present study, ZnO NPs synthesized by microwave irradiation were used for the fabrication of PCL/ZnO-NP nanocomposite via electrospinning method.

2. Materials and Method

2.1. Materials

Polycaprolactone (PCL, Mn = 70,000–90,000) and sodium hydroxide (NaOH) were obtained from Sigma–Aldrich Chemicals. Glacial acetic acid (AA), formic acid (FA), zinc nitrate hexahydrate (Zn $(NO_3)_2$ $6H_2O$) and soluble starch were purchased from Merck. All the reagents were of analytical grade and they were used without further purification.

2.2. Preparation of ZnO nanoparticles

The ZnO NPs were synthesized by the microwave method using Zn $(NO_3)_2$ $6H_2O$ and NaOH as precursors and soluble starch as a stabilizing agent. Starch was dissolved in distilled water at 87°C. 10 ml, 1M of Zn $(NO_3)_2$ $6H_2O$ solution was added to the starch solution. The obtained solution was stirred continuously using the magnetic stirrer for 15 minutes until complete dissolution occurs. Subsequently, 2M NaOH solution was added drop by drop to adjust pH= 7 of the solution. By the addition of NaOH the aqueous clear solution turned into a milky white without any precipitation. The solution was homogenized by using a Hielscher UP200 HT ultrasonic homogenizer before microwave treatment to improve nanoparticle distribution. Following this step, the solution was placed under microwave irradiation by using a domestic microwave oven operated at 600 W and 2 minutes with a frequency of 2450 MHz. After the microwave irradiation, the solution was centrifuged. In order to remove the byproducts and excessive starch bound to the nanoparticles, the precipitate was washed with distilled water twice. The powder of the ZnO nanoparticles was obtained after drying at 150°C.

2.3. Preparation of PCL/ZnO-NP nanocomposite

PCL membranes containing ZnO NPs and neat PCL were prepared by electrospinning using 15 wt. % PCL in co-solvent of AA:FA (ratio of 1:1 v/v). ZnO NPs were first dispersed in a co-solvent of AA:FA at room temperature for overnight to be able to fabricate PCL/ZnO-NP nanocomposite membrane containing 10 wt.% ZnO NPs (relative to the total polymer weight). Then, a certain amount of PCL was added into the dispersion containing ZnO NPs and stirred at room temperature for overnight in order to obtain homogenous solution. PCL solution stirred at room temperature for 3 hours for the fabrication of neat PCL membrane.

Nanofibers were fabricated by using a Nanospinner 24 Touch, Inovenso Co. In the electrospinning process, the tip to collector distance was maintained at 21 cm and an electric voltage of 24 kV was applied. The feed rate of the solution was precisely controlled by a syringe pumping system which was adjusted to a flow rate of 1.5 ml h^{-1}. The electrospun nanocomposite fibers were accumulated as nonwoven mats on a grounded target wrapped with aluminum foil. All electrospinning experiments were carried out at ambient conditions.

2.4. Characterization

Scanning electron microscope (SEM) (QUANTA FEG 250) was used to measure the nanoparticle size and determine the nanoparticle shape. The surfaces of the ZnO NPs and PCL/ZnO-NP nanocomposite fibers were sputter coated (SC7620 sputter coater, Quorum Technologies Ltd, United Kingdom) with platinum for 120s prior to SEM investigations. For each experiment, the average nanoparticle and nanofiber diameters were analyzed by the help of an image visualization software (Image-J, National Institute of Health, USA) from about 50 measurements of the random nanoparticles and nanofibers. X-ray Diffraction (XRD-PANalytical XPert Pro) analysis was conducted to prove ZnO NPs production and the presence of ZnO NPs in the PCL nanofiber. The functional groups of the ZnO NPs and the PCL nanocomposite fibers were determined by using a Fourier-transform infrared (FT-IR) spectroscopy. FT-IR spectra were collected using a spectrometer (Spectrum 100, Perkin Elmer) with 4 cm^{-1} resolution in transmittance mode in the mid-IR region (4000–650 cm^{-1}). The in vitro studies were carried out in a phosphate buffered saline (PBS) solution for time periods of 1, 2, 4 and 7 days

to determine the amount of Zn ion release from PCL/ZnO-NP nanocomposite. Fabricated nanocomposite were cut to 1x1 cm^2 area and were placed in a 10 ml PBS solution (pH=7.4). The release studies were carried out at 37 °C. The amount of Zn ions present in the PBS was determined by using a inductively coupled plasma–mass spectrometer (ICP-MS, Perkin Elmer Optima 2100 DV model).

3. Results

SEM investigations were conducted on nanoparticles and nanofibers to evaluate the morphology and size distribution of them. Representative morphological features and size of the ZnO NPs, neat PCL nanofiber and PCL/ZnO-NP nanocomposite can be seen from Figure 1. SEM images indicated that ZnO NPs were spherical in shape with an average diameter of 268±95 nm (Fig. 1 (a)). SEM micrographs, given in Fig. 1(b), revealed that the electrospun PCL nanofiber mats were composed of randomly oriented, uniform, and bead free nanofibers, with an average fiber diameter of 479±170 nm. On the other hand, nanocomposite fiber mats were also successfully generated without any beads through the electrospinning process (Figs. 1(c) and (d)). The average diameter of PCL/ZnO-NP nanocomposite fiber mat is 372±198 nm. ZnO NPs also can be seen clearly from Figs. 1(c) and (d). These results indicated that the introduction of ZnO NPs into the PCL nanofiber decreased the fiber diameter.

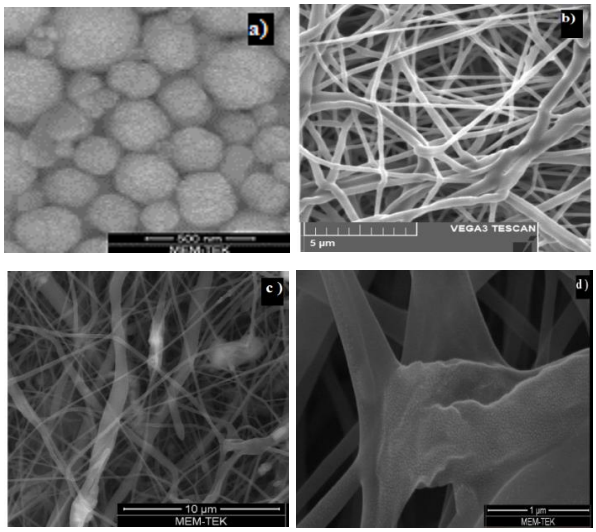

Figure 1. SEM images of the ZnO NPs (a), neat PCL nanofiber (b) and PCL/ZnO-NP nanocomposite (c and d)

The XRD patterns of the ZnO NPs and PCL/ZnO-NP nanocomposite were given in Figure 2. As can be seen from Fig. 2(a), peaks at 2θ = 32.25°, 34.87°, 36.77°, 47.99°, 57.26°, 63.27°, 66.75° and 68.24° confirmed the formation of ZnO NPs (Zhang et al., 2011). The peaks at 2θ =33.47° and 36.65° which can be seen from Fig. 2(b) show the presence of ZnO NPs in the PCL nanofiber. Moreover, the clear and sharp diffraction peaks at 2θ=21.92° and 24.23° are evidence of semi-crystalline nature of neat PCL (Augustine et al., 2014). XRD studies revealed that ZnO-NPs were successfully incorporated into the PCL neat.

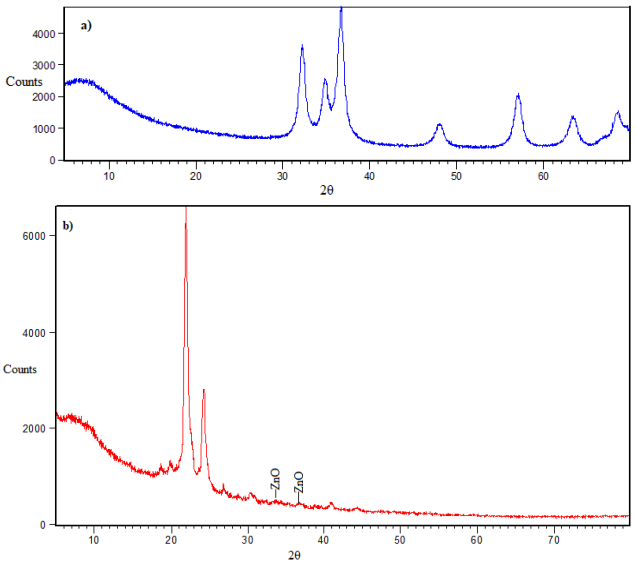

Figure 2. XRD patterns of the ZnO NPs (a) and PCL/ZnO-NP nanocomposite (b).

Figure 3 shows release amount of zinc ions from PCL/ZnO-NP nanocomposite to PBS for the time periods of 1, 2, 4 and 7 days. Results showed that the release of zinc ions was between 0.126–0.224 µg/ml. Possible burst release and higher concentration of zinc could be cytotoxic and provide unfavorable conditions for cell attachment and growth. Therefore, it is proposed that the slow release of zinc, as observed in PCL/ZnO-NP nanocomposite, is favorable for the possible tissue engineering applications of the present sample.

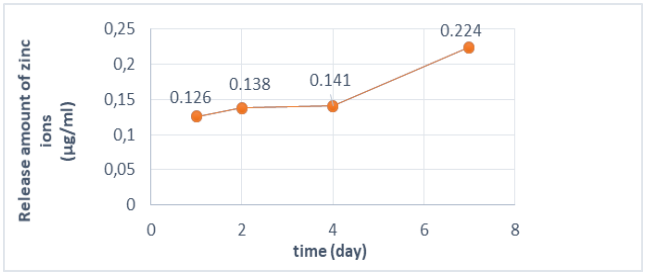

Figure 3. Release amount of zinc ions from the PCL/ZnO-NP nanocomposite in PBS solution for time periods 1, 2, 4 and 7 days.

FT-IR spectra of ZnO NPs which indicates the presence of starch in the structure of nanoparticles can be seen from Figure 4 (a). The broad absorption peaks at about 3382 and 1645 cm^{-1} are due to the hydroxyl groups of chemisorbed and/or physisorbed H_2O molecules on the particle surface. The peak at 1153 cm^{-1} was attributed to C-O bond stretching of the C-O-H group, and the peak at 1083 cm^{-1} was ascribed to C-O bond stretching of the C-O-C group in the anhydroglucose ring of starch (Zhang et al., 2011). Figure 4 (b) shows FT-IR spectra of the neat PCL nanofiber and PCL/ZnO nanocomposite. The peaks at PCL related stretching modes are represented by the peaks at 2945 cm^{-1} (asymmetric CH_2 stretching), 2867 cm^{-1} (symmetric CH_2 stretching), 1722 cm^{-1} (C=O stretching), 1294 cm^{-1} (C–O and C–C stretching), and 1238 cm^{-1} and 1164 cm^{-1} corresponding to C–O–C

asymmetric and symmetric stretching vibrations (Gomes et al., 2015; Xue et al., 2015). The PCL/ZnO-NP nanocomposite and neat PCL nanofiber presented the same spectra in the wave number range of 700–3.100 cm^{-1}.

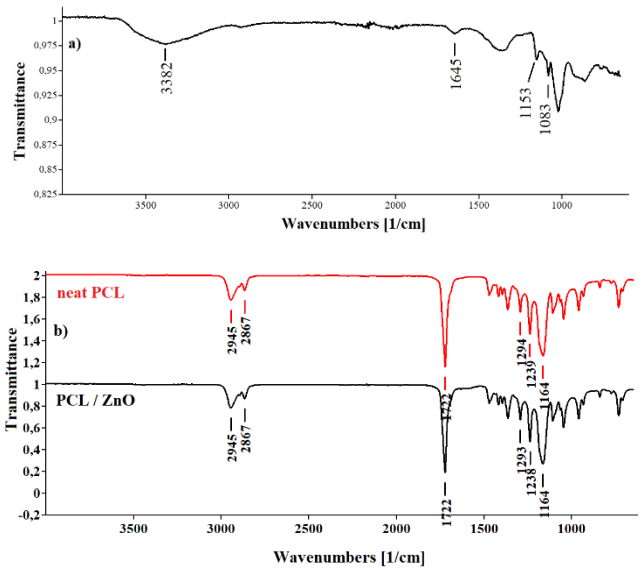

Figure 4. FT-IR spectra of the ZnO NPs (a), FT-IR spectra of the neat PCL nanofiber and PCL/ZnO-NP nanocomposite (b)

4. Discussion

ZnO NPs were successfully synthesized by microwave assisted hydrothermal method with short reaction time, low cost and very simple compared to the conventional methods. Using the water as solvent in the synthesis of ZnO nanoparticles resulted to an immediate agglomeration due to the high polarity of water. The presence of starch in the reaction medium provides to produce nanoparticles in spherical shape and helps to reduce the agglomeration (Hasanpoor et al., 2015; Zhang et al., 2011).

SEM image of neat PCL nanofiber indicated that the fibers had smooth surface. The surface of PCL/ZnO-NP nanocomposite was rough due to the agglomeration of ZnO NPs. SEM images of neat PCL nanofiber and PCL/ZnO-NP nanocomposite indicated that ZnO NPs in the fibers caused to decrease of the fiber diameter. It was thought that the reason of the decreasing the diameter of the fibers containing ZnO NPs was that the addition of the ZnO NPs into spinning solution leads to increase in the electrical conductivity of the solution. The increase in conductivity of the solution can increase the electric charge density on the surface of the ejected spinning jet. Thus, the increasing charge density of spinning jet can decrease self-repulsion tension and increase elongation forces. As a result of this, higher elongation forces could provide to overcome the self-repulsion tension during the electrospinning process and the diameters of the fabricated fibers can decrease. (Augustine et al., 2014; Münchow et al., 2015).

It was reported that upon the dissolution of the polymeric matrix, the controlled release of therapeutic ions brings about additional functionalities, including osteogenesis, angiogenesis, and antibacterial effects. Therefore, it is of great importance to determine the amount of therapeutic ions released from the polymeric matrix. However, high concentrations of these ions can cause free radical formation and cytotoxicity. Thus, it is necessary to control the release of zinc ions at a clinically acceptable rate. Lee et al., who studied dose-dependent cytotoxicities after the treatment with ZnO nanoparticles in human epidermal keratinocyte HaCaT cells stated that the amount of zinc ions released from ZnO nanoparticles (~20 nm, spherical shape and hydrodynamic size were 986±46 nm) as 10, 20, 40 and 80 µg/mL for the time periods of 6, 12 and 24 h. At the dosage of 10 µg/mL, approximately 100% cell viability was observed for 24 h. Although, at the dosage of 20 µg/mL, viability of cell decreased with the exposure time dependence, viability of cell was found to be greater than 50% for 24 h. At 40 and 80 µg/mL doses, significant differences in cell viability were observed below 50% for 24 h (Lee et al., 2012). In our study, the release amount of zinc ions was below than the values in that study. PCL/ZnO-NP nanocomposite can be considered as non-toxic to the skin.

It was reported in the literature that ZnO NPs displayed antibacterial activity and enhanced cell proliferation/wound healing (Augustine et al., 2014; Münchow et al., 2015). As mentioned before, ZnO NPs serve as a sustained ionic Zn source best suited for topic wound application by enhancing re-epithelialization, decreasing inflammation and bacterial growth. It is considered that the fabricated material can be used as a wound dressing material due to ZnO NPs were successfully incorporated into the PCL fiber and the release of zinc ions from the PCL/ZnO-NP nanocomposite has been observed.

5. Conclusions

In this study, ZnO NPs and electrospun PCL scaffolds incorporated with ZnO NPs were successfully fabricated and characterized. SEM and XRD analysis revealed the presence of ZnO NPs in the fibers. These findings indicated that the currently described electrospun nanocomposite fiber mats are very promising materials as they combine the high biocompatability of PCL, the beneficial effects of zinc ions on antibacterial properties and an interconnected porous structure of electrospun nanofibers that may allow cell adhesion, cell invasion and vascularization. It is believed that the PCL nanocomposite mat incorporated with the wound healing and antibacterial properties provided by ZnO NPs has potential to be used in wound dressing applications.

Acknowledgements

This work was supported by Istanbul Technical University Scientific Research Office (BAP). Project number is MYL-2018-41501.

References

Augustine R, Malik HN, Singhal DK, Mukherjee A, Malakar D, Kalarikkal N, Thomas S 2014. Electrospun polycaprolactone/ZnO nanocomposite membranes as biomaterials with antibacterial and cell adhesion properties. Journal of Polymer Research, 21(347): 1-18.

Faal Hamedani N, Farzaneh F 2006. Synthesis of ZnO Nanocrystals with Hexagonal (Wurtzite) Structure in Water Using Microwave Irradiation, Journal of Sciences, Islamic Republic of Iran 17(3): 231-234.

Gomes SR, Rodrigues G, Martins GG, Roberto MA, Mafra M, Henriques CMR, Silva JC 2015. In vitro and in vivo evaluation of electrospun nanofibers of PCL, chitosan and gelatin: A comparative study, Mater. Sci. Eng. C 46:348–358.

Hasanpoor M, Aliofkhazraei M, Delavari H 2015. Microwave-assisted synthesis of zinc oxide nanoparticles, Procedia Materials Science 11:320 – 325.

Król A, Pomastowski P, Rafińska K, Railean-Plugaru V, Buszewski B 2017. Zinc oxide nanoparticles: Synthesis, antiseptic activity and toxicity mechanism, Advances in Colloid and Interface Science 249:37–52.

Lansdown ABG, Mirastschijski U, Stubbs N, Scanlon E, Agren MS 2007. Zinc in wound healing: theoretical, experimental, and clinical aspects, Wound Repair Regen. 15(1): 2-16.

Lee SH, Lee R, Kim Y, Kim M 2012. Toxic Response of Zinc Oxide Nanoparticles in Human Epidermal Keratinocyte HaCaT Cells, Toxicol. Environ. Health. Sci 4(1): 14-18.

Liu M, Duan X, Li Y, Yang D, Long Y 2017. Electrospun nanofibers for wound healing. Materials Science and Engineering C 76: 1413–1423.

Mogoşanu GD, Grumezescu AM 2014. Natural and synthetic polymers for wounds and burns dressing. International Journal of Pharmaceutics 463: 127– 136.

Münchow EA, Albuquerque MTP, Zero B, Kamocki K, Piva E, Gregory RL, Bottino MC 2015. Development and characterization of novel ZnO-loaded electrospun membranes for periodontal regeneration. Dental Materials 31: 1038–1051.

Premanathan M, Karthikeyan K, Jeyasubramanian K, Manivannan G 2011. Selective toxicity of ZnO nanoparticles toward Gram-positive bacteria and cancer cells by apoptosis through lipid peroxidation, Nanomedicine: Nanotechnology, Biology, and Medicine 7: 184–192.

Rath G, Hussain T, Chauhan G, Garg T, Goyal AK 2016. Development and characterization of cefazolin loaded zinc oxide nanoparticles composite gelatin nanofiber mats for postoperative surgical wounds, Materials Science and Engineering C 58: 242–253.

Shoja M, Shameli K, Ahmad MB, Kalalntarı K 2015. Preparation, characterization and antibacterial properties of Polycaprolactone/ZnO microcomposites. Digest Journal of Nanomaterials and Biostructures 10(1): 169-178.

Toduka Y, Toyooka T, Ibuki Y 2012. Flow Cytometric Evaluation of Nanoparticles Using Side-Scattered Light and Reactive Oxygen Species-Mediated Fluorescence−Correlation with Genotoxicity, Environ. Sci. Technol.46: 7629−7636.

Wei Q, Xu F, Xu X, Geng X, Ye L, Zhang A, Feng Z, 2016. The multifunctional wound dressing with core–shell structured fibers prepared by coaxial electrospinning. Front. Mater. Sci. 10(2): 113–121.

Xue J, Shi R, Niu Y, Gong M, Coates P, Crawford A, Chen D, Tian W, Zhang L 2015. Fabrication of drug-loaded anti-infective guided tissue regeneration membrane with adjustable biodegradation property, Colloids and Surfaces B: Biointerfaces 135: 846–854.

Zhang G, Shen X, Yang Y 2011. Facile Synthesis of Monodisperse Porous ZnO Spheres by a Soluble Starch-Assisted Method and Their Photocatalytic Activity, The Journal of Physical Chemistry C 115: 7145–7152.

Eurasian J. Bio. Chem. Sci. 1(2): 59-62, 2018

EJBCS

Eurasian Journal of Biological and Chemical Sciences

Journal homepage: www.dergipark.gov.tr/ejbcs

Conductivity, Dielectric And Modulus Studies of Methylcellulose-NH_4TF Polymer Electrolyte

M. S. M. Misenan[1], *A. S. A. Khiar[2]

[1,2] *Universiti Sains Islam Malaysia, Faculty of Science and Technology, Nilai, Malaysia*

*Corresponding author : azwanisofia@usim.edu.my
Orcid No: 0000-0002-0014-1247

Abstract: Solid biopolymer electrolyte based on methylcellulose (MC) were prepared with different weight percentage of ammonium triflate (NH4TF) salt via solution casting technique. The film was characterized by impedance spectroscopy to measure its ionic conductivity. Samples with 45% of NH_4TF exhibit the highest conductivity of 1.14 x 10^{-4} S cm^{-1}at ambient. Dielectric data were analysed using complex permittivity and complex electrical modulus for the sample with highest conductivity. Dielectric data proved that the increase in conductivity is mainly due to the increase in number of charge carriers.

Keywords: Solid biopolymer electrolyte; Methyl Cellulose; salt; conductivity.

1. Introduction

Electrolyte is a substance concentrated with free ionic species, which behaves as an electrically conductive medium. It can be divided into a few categories based on its physical condition. However, there are a few obstacles that had been faced by liquid electrolytes which limit its performance. Such limitations are corrosion reactions between separator and electrodes, high tension during battery assembly operation, leakage of the harmful aqueous electrolytes that requires special sealing and packaging (Shanti, 2011). To overcome the problem associated with liquid electrolytes, scientist proposed a new electrolyte which is polymer electrolyte.

Polymer electrolyte basically is defined as solid ionic conductors formed by the dissolution of salts in suitable high molecular weight polymers (Vincent, 1987). It can be divided into few types which are gel, composites and solid. According to Buraidah and Arof (2011) polymer electrolytes have attracted much attention due to their potential applications in electrochemical devices such as rechargeable batteries, fuel cells, super capacitors and solar cells.

Since conductivity is the main focus for polymer electrolytes, many research have been conducted to study its conductivity. There are many ways to improve conductivity of polymer electrolytes such as polymer blending, plasticization, and mixed salts systems (Misenan et al., 2018; Buraidah & Arof, 2011; Kadir et al., 2009).

In the present work, methyl cellulose has been chosen as the host polymer. Methylcellulose is a chemical compound from cellulose. Generally, cellulose derivatives are polysaccharides composed of linear chains of (1-4) glucosidic units of methyl, hydroxypropyl or carboxyl substituents. Pinotti et al. (2007) stated that the advantages of using methylcellulose in producing polymer electrolyte is that it have efficient oxygen and lipid barrier properties. From literature, it is reported that, MC – ammonium fluoride (NH_4F) obtained the highest conductivity of $6.40x10^{-7}$ Scm^{-1} (Nik Aziz et al., 2010) and MC-ammonium nitrate (NH_4NO_3) obtained a room temperature conductivity of 2.10×10^{-6} S cm^{-1} (Suhaimi et al., 2010). Consequently, by doping ammonium iodide (NH_4I) with MC electrolyte give the highest conductivity at 5.08 x 10^{-4} Scm^{-1} (Salleh et al., 2016).

Additionally, earlier study was reported that, methyl cellulose/chitosan blend polymer doped with ammonium triflate (NH_4TF) has obtained optimum conductivity of 4.99 x 10^{-6} Scm^{-1} (Hamdan & Khiar, 2013). In this report methyl cellulose as single polymer host is dope with the NH_4TF salt to study the correlation between the concentration of salt doped in polymer electrolyte and its conductivity value.

2. Materials and Method

2.1. Sample Preparation

Methyl cellulose solution doped with various amount of ammonium triflate, NH4TF salt were prepared by solution

casting technique. 0.5 g of methyl cellulose was dissolved in 50 mL distilled water. An amount of 10 w.t%, 15w.t%, 20w.t%, 25w.t%, 30w.t%, 35w.t%, 40w.t%, 45w.t% and 50w.t% of NH4TF was added into the solution. The solution was further stirred homogenously and then casted onto plastic petri dish and left to dry at room temperature before further analysis. The composition and their label is tabulated in table 1.

Table 1: Composition of biopolymer electrolyte with their tagging.

Ammonium triflate (NH_4TF), weightage	Label
10	10 SALT
15	15 SALT
20	20 SALT
25	25 SALT
30	30 SALT
35	35 SALT
40	40 SALT
45	45 SALT
50	50 SALT

2.2 Conductivity Measurement.

The conductivity of the sample was measured by using Impedance Spectroscopy via HIOKI 3532 LCR Hi Tester Bridge interfaced to a computer. The impedance values were measured within the frequency of 50Hz to 1MHz at ambient temperature. A negative imaginary impedance, *Zi* versus real impedance, *Zr* with same scale of horizontal and vertical axes were then plotted where the bulk resistance, *Rb* could be obtained. Hence, the conductivity of the sample in room temperature can be calculated by using equation (1):

$$\sigma = t / Rb\, A \qquad (1)$$

Where *Rb* is bulk resistance, *t* is the thickness of the thin film and *A* is the surface area of contact. In order to measure the thickness of the thin film, a digital micro meter screw gauge was used. **3. Results and Discussion**

Figure 1 shows a typical cole-cole plot for methyl cellulose polymer doped with various concentration of NH_4TF. The complex impedance plot generated by impedance measurement basically consist of (i) a title spiked, (ii) a depressed semicircle or (iii) a combination of depressed semicircle and title spike (Kaith et al., 2014). From the plot, it can observed that for polymer electrolyte with lower concentration of salt mostly shows a combination of depressed semicircle and a spike. While for higher concentration of salt, the polymer electrolyte exhibits inclination of spike line with real impedance axis, Zr.

Additionally, the bulk electrical resistance (Rb) is interpreted from the intercept of semicircle curves and spike lines with the real impedance (Zr) axis. Ariffin and Khiar (2015) stated that the conduction of ions in the bulk of polymer electrolyte exhibits semicircles while the spike line is caused by the effect of electrode polarization which is a characteristic of diffusion process.

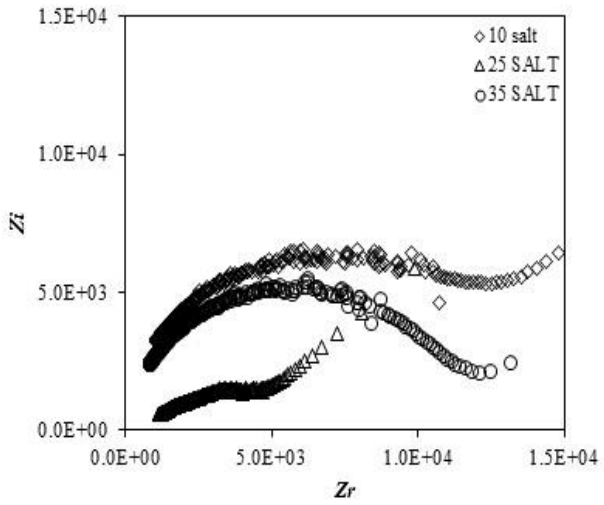

Figure 1. Impedance plot at ambient temperature. Onset Fig shows the impedance plot for the highest conducting sample.

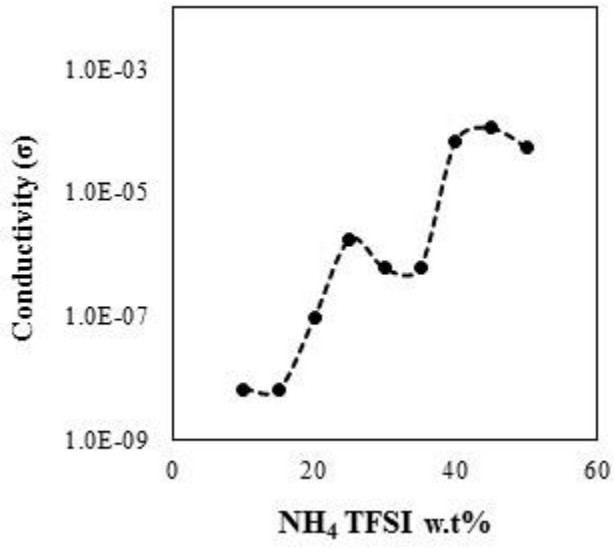

Figure 2. Variation of ionic conductivity as a function of NH4TF concentration

Figure 2. shows that the conductivity plot for methyl cellulose electrolyte with different amount of ammonium triflate.

The addition of NH_4TF doping introduces free ammonium cation (NH_4^+) and free triflate anion ($CF_3SO_3^-$) to be dissociated. The dissociated cation occurs when

incorporation salt interact with functional group of polymer host. From the plot, it can be observed that the conductivity increases up to 1.14 x 10 $^{-4}$ Scm^{-1} with addition of 45 w.t% NH_4TF salt. This is due to the increase in the number of mobile ion in the polymer electrolyte system and also the amorphousness of the polymer is increase, hence reduces the energy barriers which enhance the mobility of the ion (Sahli & Ali, 2012). Nevertheless, the conductivity decreased beyond the 45 w.t% of NH_4TF doped polymer electrolyte due to the accumulation of ion cluster, which provide an overcrowded ions environment in the polymer salt system (Hafiza et al., 2017).

The dielectric studies can be the best way to describe the conductivity behaviour of polymer electrolytes. Dielectric constant εr charge carrier, n and the dissociation energy, *U* are related to the equation:

$$\eta = \eta_0 \exp(-U/(\varepsilon r\, kT)) \quad (2)$$

From this equation, it can be described that, when the dielectric constant, εr increases, the number of charge carriers increases. In polymer electrolytes, ions are the charge carriers where the dielectric constant represent the stored charge in material (Buraidah et al., 2009). The dielectric constant εr and its imaginary part of complex permitivity is given by:

$$\varepsilon r = Zi / \omega C_0 (Zr^2 + Zi^2) \quad (3)$$

$$\varepsilon i = Zr / \omega C_0 (Zr^2 + Zi^2) \quad (4)$$

Where $Co = \varepsilon oA/t$ where εo is the permittivity of the free space, *A* is the area of the sample and t is the thickness of the sample and ω is equal to $2\pi f$, which *f* in frequency taken from the data in Hz.

Figure 3 (a) and (b) shows the real part, εr and imaginary part, εi of dielectric constant at selected w.t% of salt content. The observation from the graph shows that the real part of dielectric constant, εr increases with increasing salt content for respective frequencies until 45 w.t% where beyond that the εr value decreases. This is because of the increase in number density of mobile ions as when the composition of salt increases the stored charge of the sample increases (Buraidah and Arof, 2009). The dielectric constant decreases beyond 45 w.t% due to the re-association of ions. This also might be caused by the tendency of dipoles in the macromolecules to orient themselves in the direction of the applied field within low frequency range (Ibrahim et al., 2011).

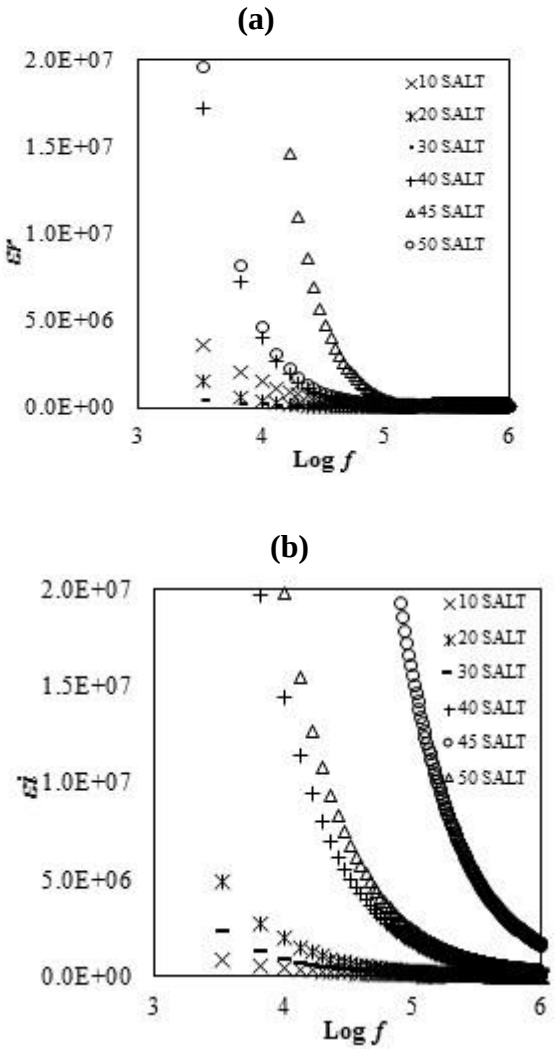

Figure 3: a) Real part of dielectric constant b) Imaginary part of dielectric constant, as a function of frequency for selected samples.

To further understand the dielectric behaviour dielectric moduli is needed which suppress the effects of electrode polarization. The equations for real electrical modulus *Mr* and imaginary modulus *Mi* can be expressed as follows:

$$Mr = \varepsilon r / (\varepsilon r^2 + \varepsilon i^2) \quad (5)$$

$$Mi = \varepsilon i / (\varepsilon r^2 + \varepsilon i^2) \quad (6)$$

Figure 4 (a) and (b) depicts the variation of real part, *Mr* and imaginary part, *Mi* of electric modulus respectively. As the frequencies increases, both of *Mr* and *Mi* also increases. At the low frequencies regions, both *Mr* and *Mi* tend towards zero values. The appearance of this long tail at low frequencies is highly attributed to the large capacitance associated with the electrodes which confirms a non-Debye behavior (Khiar at al., 2006).

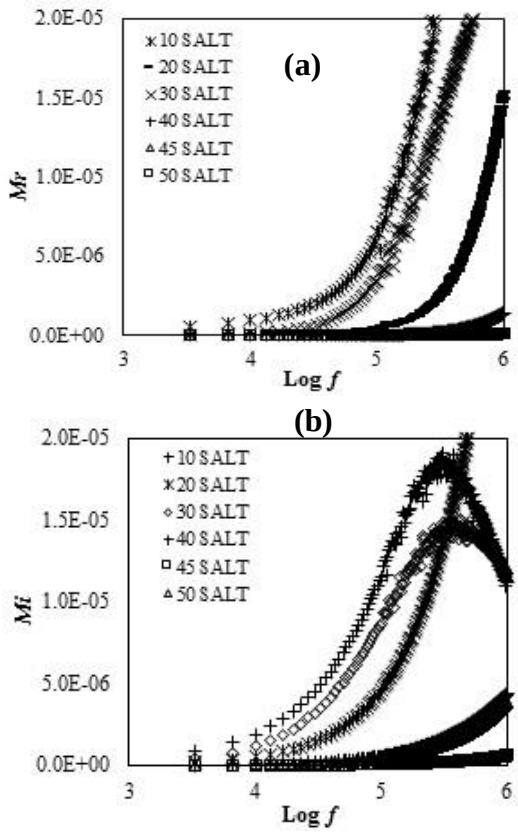

Figure 4: a) variation of real part, Mr and b) imaginary part, Mi of electric modulus as a function of frequency for 10 wt% to 50 wt% of salt content.

5. Conclusions

Solid polymer electrolyte from methyl cellulose with different weight percentage of NH_4TF (10 to 50 wt%) has been prepared via solution casting technique. The addition of NH_4TF gradually increases the ionic conductivity of polymer electrolyte with a maximum conductivity of 1.14 x 10^{-4} S cm^{-1} was achieved at 45 wt% of NH_4TF. The tendencies of dielectric constant, over the concentration of NH_4TF propose that the number of charge carriers strongly influences the increase in conductivity.

Acknowledgements

This work was funded by FRGS under vote USIM/FRGSFST-32-51312. The authors would like to thank Faculty of Science and Technology, Universiti Sains Islam Malaysia for the facilities provided.

References

Ariffin N. A., A. S. A. Khiar. 2015. Effect of BMITFSI to the Electrical Properties of Methylcellulose/ Chitosan/ NH_4TF Based Polymer Electrolyte. Proc. of SPIE.9668.

Buraidah, M. H., A. K. Arof. 2011. Characterization of Chitosan/PVA Blended Electrolyte Doped with NH_4I. Journal of Non-Crystalline Solids, 357:3261-3266.

Buraidah, M. H., L.P. Teo, S.R. Majid, A.K. Arof. 2009. Ionic Conductivity by Correlated Barrier Hopping of NH_4I Doped Chitosan Solid Electrolyte. Physica B, 404:1373-1379.

Hafiza, M. N., & Isa, M.I.N., Solid polymer electrolyte production from 2-hydroxyethyl cellulose: Effect of NH_4NO_3 composition on its structural properties. Carbohydrate Polymers http://dx.doi.org/10.1016/j.carbpol.2017.02.03.

Hamdan K Z, A. S A Khiar. 2014. Conductivity and Dielectric Studies of Methylcellulose/Chitosan-$NH_4CF_3SO_3$ Polymer Electrolyte. Key Engineering Materials, 594-595: 818-822.

Ibrahim S., S.M. Mohd Yasin, N.M. Nee, R. Ahmad, M.R. Johan. 2011. Conductivity and dielectric behaviour of PEO-based solid nanocomposite polymer electrolytes. Solid StateCommunications, doi:10.1016/j.ssc.2011.11.037.

Kadir M. F. Z., L.P. Teo, S.R. Majid, A.K. Arof. 2009. Conductivity studies on plasticized PEO/chitosan proton conducting polymer electrolyte, Materials Research Innovations, 13:191-194.

Kaith Balbir S., Reena Sharma, Susheel Kalia and Manpreet S. Bhatti. 2014 Response surface methodology and optimized synthesis of guar gum-based hydrogels with enhanced swelling capacity. Royal Society of Chemistry Advanced 4: 40339.

Khiar, A.S.A., R.Puteh, A.K. Arof. 2006. Conductivity Studies of a Chitosan-Based PolymerElectrolyte. Physica B. 373:23-27.

Misenan, M. S. M. M. I. N. Isa, A. S. A. Khiar. 2018. Electrical and structural studies of polymer electrolyte based on chitosan/methyl cellulose blend doped with BMIMTFSI. Materials Research Express 5: https://doi.org/10.1088/2053-1591/aac25b.

Nik Aziz N.A, N. K. Idris, & M. I. N. Isa. 2010. Solid polymer electrolytes based on methylcellulose: FT-IR and ionic conductivity studies. International Journal of Polymer Analysis and Characterization, 15(5): 319-327.

Pinotti A, M A Garcia, M N Martino, N E Zarithzky. 2007. Study on microstructure and physical properties of composite films based on chitosan and methylcellulose. Food Hydrocolloids, 21:66-72.

Sahli N. and A. M. M. Ali. 2012. Effect of Lithium Triflate Salt Concentration in Methyl Cellulose based Solid Polymer Electrolytes. IEEE Colloquium on Humanities, Science & Engineering Research.

Salleh N. S., Shujahadeen B. Aziz, Z. Aspanut, M. F. Z. Kadir. 2016 .Electrical impedance and conduction mechanism analysis of biopolymer electrolytes based on methyl cellulose doped with ammoniumiodide. Ionics. DOI 10.1007/s11581016-1731-0.

Shanti, R. 2011. Invstigation on the Effects of Ionic Liquid and Ionic Mixture in Biodegradable Polymer Electrolytes. Master of Science Thesis. University Tunku Abdul Rahman.

Shuhaimi N. E. A., L.P. Teo, S.R. Majid, A.K. Arof. 2010. Transport studies of NH4NO3 doped methyl cellulose electrolyte. Synthetic Metals, 160: 1040–1044.

Vincent C. A. 1987. Polymer Electrolytes. Progress in Solid State Chemistry, 17:145-261.

EJBCS